nature medicine

LETTERS

https://doi.org/10.1038/s41591-019-0498-z

# Programmable bacteria induce durable tumor regression and systemic antitumor immunity

Sreyan Chowdhury[1,2], Samuel Castro[1], Courtney Coker[1], Taylor E. Hinchliffe[1], Nicholas Arpaia[2,3*] and Tal Danino[1,3,4*]

**Synthetic biology is driving a new era of medicine through the genetic programming of living cells[1,2]. This transformative approach allows for the creation of engineered systems that intelligently sense and respond to diverse environments, ultimately adding specificity and efficacy that extends beyond the capabilities of molecular-based therapeutics[3–6]. One particular area of focus has been the engineering of bacteria as therapeutic delivery systems to selectively release therapeutic payloads in vivo[7–11]. Here we engineered a non-pathogenic *Escherichia coli* strain to specifically lyse within the tumor microenvironment and release an encoded nanobody antagonist of CD47 (CD47nb)[12], an anti-phagocytic receptor that is commonly overexpressed in several human cancer types[13,14]. We show that delivery of CD47nb by tumor-colonizing bacteria increases activation of tumor-infiltrating T cells, stimulates rapid tumor regression, prevents metastasis and leads to long-term survival in a syngeneic tumor model in mice. Moreover, we report that local injection of CD47nb-expressing bacteria stimulates systemic tumor-antigen-specific immune responses that reduce the growth of untreated tumors, providing proof-of-concept for an abscopal effect induced by an engineered bacterial immunotherapy. Thus, engineered bacteria may be used for safe and local delivery of immunotherapeutic payloads leading to systemic antitumor immunity.**

The origins of cancer immunotherapy trace back to the pioneering work of William Coley, who observed tumor clearance in some patients that received injections of bacteria[15]—a result that has now been attributed to leukocyte activation[16–18]. Several studies have demonstrated that bacteria preferentially grow within tumor cores owing to the immunoprivileged nature of the often hypoxic and necrotic tumor microenvironment, and can locally affect tumor growth through the recruitment and activation of the immune system[19–23]. With the advent of synthetic biology over the past two decades and the development of numerous bacterial gene circuits[6,24–28], we reasoned that programming bacteria to controllably release recombinant immunotherapies could enable the local delivery of higher effective concentrations of therapy while preventing the toxicities observed following systemic delivery of identical or similar therapeutic agents.

To test this approach, we chose to target CD47, an anti-phagocytic receptor that is overexpressed in several human cancer types[13,14,29]. Recent studies have demonstrated that CD47 blockade not only increases phagocytosis of cancer cells but also promotes cross-presentation of tumor antigens to enhance priming of antitumor effector T cells in syngeneic mouse tumor models[12,30–32]. However, as demonstrated in both preclinical models[33] and human trials[34,35], systemic CD47 blockade can result in anemia and thrombocytopenia due to the high expression of CD47 on red blood cells and platelets, respectively. To improve its therapeutic profile, a nanobody (a camelid single-domain antibody fragment) against CD47 with an approximately 200-fold higher binding affinity than commercially available anti-mouse CD47 monoclonal antibodies was recently developed and characterized[12]. This nanobody demonstrated mild effects as a monotherapy, potentially due to the lack of Fc-mediated effector function[33,36]; however, a notable therapeutic response was observed when used in combination with a tumor-specific antibody and systemic immune-checkpoint blockade. Here, we engineered an *E. coli* strain, which contained a synchronized lysis circuit (eSLC), that colonizes tumors and undergoes intratumoral quorum lysis to locally release an encoded nanobody antagonist of CD47 (eSLC–CD47nb) (Fig. 1a). This system allows for the combined local delivery of an immunotherapeutic agent along with immunostimulatory bacterial lysis adjuvants to stimulate antitumor immunity and promote tumor regression.

To confirm expression and lysis-dependent release of CD47nb, we transformed non-pathogenic *E. coli* with a single plasmid that encodes the eSLC, as well as a stabilized plasmid that drives constitutive expression of a hemagglutinin (HA)-tagged variant of CD47nb (Extended Data Fig. 1). The SLC$^+$ strain grows and produces the quorum-sensing molecule acylhomoserine lactone through the expression of *luxI* and lyses at a critical threshold owing to the production of a bacteriophage lysis protein (ϕX174E), resulting in bacterial death and therapeutic release[8] (Fig. 1a). As this gene circuit was previously tested using two plasmids of differing copy numbers[8], we verified SLC-mediated lysis of eSLC–CD47nb *E. coli* using time-lapse microscopy of bacteria using an agar pad[37]. eSLC–CD47nb grew, reached quorum and lysed over a 20-h time course, in contrast to non-SLC *E. coli* (SLC$^-$), which continuously grew and filled the field of view (Extended Data Fig. 2a). Furthermore, we cultured SLC$^+$ and SLC$^-$ *E. coli* in lysogeny broth (LB) medium in a 96-well plate and measured the optical density at 600 nm ($OD_{600}$) over time. eSLC–CD47nb-expressing *E. coli* (SLC$^+$) exhibited multiple periodic dips in $OD_{600}$, indicating rounds of synchronized lysis, whereas SLC$^-$ *E. coli* exhibited normal bacterial growth kinetics (Fig. 1b). After verifying the synchronized lysis behavior, we evaluated lysis-mediated release of CD47nb in batch cultures. Immunoblots of log-phase bacterial cultures indicated that eSLC–CD47nb bacteria released significantly higher levels of HA-tagged CD47nb into culture supernatants than control CD47nb–HA

[1]Department of Biomedical Engineering, Columbia University, New York, NY, USA. [2]Department of Microbiology and Immunology, Vagelos College of Physicians and Surgeons, Columbia University, New York, NY, USA. [3]Herbert Irving Comprehensive Cancer Center, Columbia University, New York, NY, USA. [4]Data Science Institute, Columbia University, New York, NY, USA. *e-mail: na2697@cumc.columbia.edu; td2506@columbia.edu

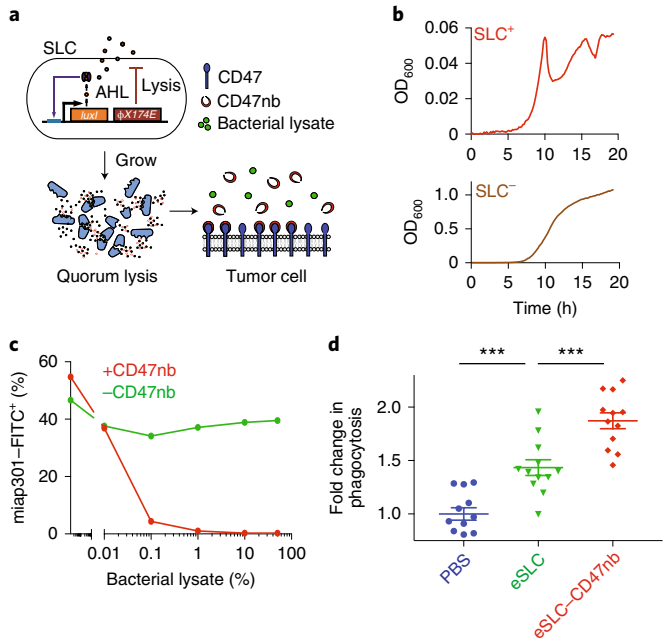


**Fig. 1 | Quorum-induced release of functional anti-CD47 blocking nanobody by engineered immunotherapeutic bacteria encoding a SLC.** **a**, *E. coli* with SLC reach a quorum and induce the phage-lysis protein ϕX174E, leading to bacterial lysis and release of a constitutively produced, anti-CD47 blocking nanobody that binds to CD47 on the tumor cell surface. **b**, Bacterial growth dynamics over time of SLC$^+$ and SLC$^-$ *E. coli* in batch liquid culture. Data are representative of three independent experimental replicates. **c**, A20 cells were co-incubated with a fixed concentration of FITC-conjugated anti-CD47 monoclonal antibody (FITC–miap301) along with serial dilutions of bacterial lysates that contained constitutively expressed CD47nb (pSC02) or empty vector (pSC03). Data are representative of two independent experimental replicates. **d**, In vitro phagocytosis of DiI-labeled A20 cells pretreated with PBS or lysates of SLC$^+$ or SLC$^+$CD47nb$^+$ bacteria by BMDMs ($n=4$ fields of view of three replicates, $^{***}P=0.0003$, one-way analysis of variance (ANOVA) with Bonferroni's multiple comparisons test). Data are mean ± s.e.m.

bacteria without SLC (Extended Data Fig. 2b), suggesting that CD47nb release is enhanced by eSLC.

To verify that the bacterially produced nanobody functionally binds to CD47, A20 lymphoma cells—which are known to express CD47[30]—were incubated with a fixed concentration of fluorescein isothiocyanate (FITC)-labeled anti-mouse CD47 monoclonal antibody (clone miap301) and serial dilutions of bacterial lysates from eSLC–CD47nb or eSLC bacteria containing an empty vector (Fig. 1c and Extended Data Fig. 2c). We observed a progressive reduction in CD47 staining when cells were incubated with lysates from bacteria expressing CD47nb, suggesting that bacterially produced CD47nb could outcompete miap301 binding to CD47 on the surface of A20 cells. We additionally cloned a C-terminal 6×His-tagged variant of CD47nb and purified recombinant CD47nb (rCD47nb) by nickel-affinity chromatography. Similarly, we observed a progressive reduction in FITC fluorescence when A20 cells were co-incubated with increasing concentrations of rCD47nb and a fixed concentration of FITC-labeled miap301 (Extended Data Fig. 2d).

Moreover, we evaluated the ability of eSLC–CD47nb to induce A20 tumor cell phagocytosis by bone-marrow-derived macrophages (BMDMs) (Fig. 1d and Extended Data Fig. 2e). As expected, treatment with anti-CD47 monoclonal antibody resulted in a 60% increase in phagocytosis (Extended Data Fig. 2e) and treatment with eSLC lysate alone led to an increase in phagocytosis of tumor cells by 50%. Notably, eSLC–CD47nb lysate treatment led to a 90% increase in phagocytosis compared to baseline, indicating that eSLC–CD47nb enhances phagocytosis of tumor cells by macrophages in a combinatorial, dose-dependent manner—through CD47 blockade as well as TLR agonism due to bacterial lysis adjuvants (Fig. 1d and Extended Data Fig. 2e). Overall, these results indicate that eSLC–CD47nb releases CD47nb in a lysis-dependent manner and that CD47nb can induce phagocytosis of tumor cells by BMDMs in vitro.

We next sought to evaluate the clinical efficacy of eSLC–CD47nb bacteria in a syngeneic mouse model. BALB/c mice bearing A20 tumors in both hind flanks received intratumoral injections of PBS, eSLC bacteria or eSLC–CD47nb bacteria. Although administration of control eSLC alone initially slowed tumor growth, likely owing to the activation of innate immune cells by bacterial products released upon quorum lysis, final tumor volumes were not statistically different from PBS-treated mice. By contrast, administration of eSLC–CD47nb resulted in rapid and durable clearance of established A20 tumors within approximately 10 days of commencing therapy (Fig. 2a and Extended Data Fig. 3a,b). In contrast to animals that received intratumoral injections of PBS or control eSLC bacteria, liver metastases were rarely observable in mice treated with eSLC–CD47nb at 30 days after treatment (Fig. 2b). Notably, approximately 80% of mice treated with eSLC–CD47nb survived more than 90 days (Fig. 2c) and surviving mice were resistant to rechallenge by subcutaneous injection of $10\times10^6$ A20 cells (Fig. 2d), whereas naive mice that received the same batch of A20 cells developed tumors within a week of injection.

Subsequently, we explored the importance of therapeutic delivery of individual components of our quorum-lysis system (Fig. 2e and Extended Data Fig. 3d). First, we evaluated efficacy of CD47 blockade by intraperitoneal delivery of miap301 with or without intratumoral injection of eSLC. Neither group demonstrated significant efficacy in comparison to treatment of eSLC alone in an A20 mouse model. Although mice treated intratumorally with recombinant CD47nb or sonicated eSLC–CD47nb bacterial lysates exhibited slower tumor growth in comparison to mice treated with eSLC, complete tumor regression was only observed upon treatment with live, eSLC–CD47nb-expressing bacteria (Fig. 2e and Extended Data Fig. 3d). These data collectively suggest that continuous SLC-mediated intratumoral release of CD47nb is essential to therapeutic efficacy.

To assess the broader applicability of our approach, we also examined efficacy by intravenous administration as well as by using additional mouse tumor models. Significant therapeutic efficacy was observed when eSLC–CD47nb was intratumorally injected in other syngeneic mouse models, such as in mice bearing triple-negative breast cancer cells (4T1, Fig. 2f and Extended Data Fig. 4b) and melanoma cells (B16-F10, Fig. 2h and Extended Data Fig. 4c). Lung metastases were notably reduced in mice that received eSLC–CD47nb in the 4T1 model (Fig. 2g). We additionally explored the ability of eSLC–CD47nb to safely target and treat tumors through systemic intravenous delivery. In comparison to mice who received a systemically delivered anti-CD47 antibody (miap301), mice injected with intravenous eSLC–CD47nb showed significantly slower tumor growth (Fig. 2i and Extended Data Fig. 5a). Following treatment, bacteria localized exclusively to tumors compared to the liver, spleen and kidney (Extended Data Fig. 5b). Bacterial therapy was well-tolerated by animals, with no significant differences in body weight between treatment groups observed throughout the observation period after both intratumoral and intravenous delivery (Extended Data Figs. 3c, 4a, 5c). Overall, these results indicate that eSLC–CD47nb can safely promote local tumor regression while also preventing metastasis, suggesting the induction of systemic antitumor immunity that is likely mediated by tumor-specific T cells.

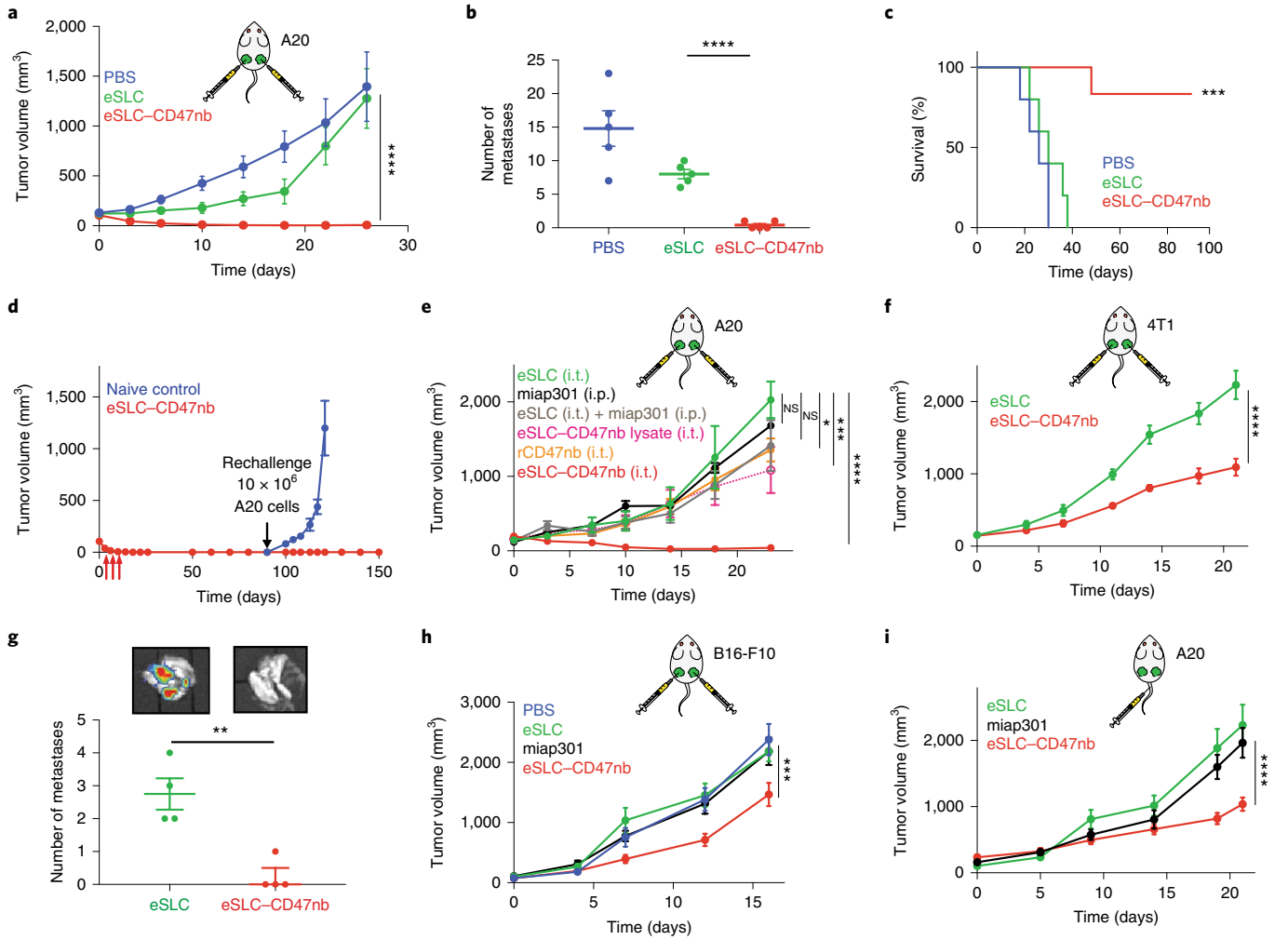


**Fig. 2 | Intratumoral production of CD47 nanobody by eSLC elicits antitumor responses in multiple syngeneic mouse tumor models. a**, BALB/c mice ($n=7$ per group) were implanted subcutaneously with $5\times10^6$ A20 B cell lymphoma cells on both hind flanks. When tumor volumes were 100–150 mm$^3$, mice received intratumoral injections every 3–4 days with PBS, eSLC or eSLC–CD47nb in both tumors. Tumor growth curves (****$P<0.0001$, two-way ANOVA with Tukey's multiple comparisons test). Data are representative of two independent experimental replicates. Tumor growth curves of tumors from individual mice are shown in Extended Data Fig. 3a. **b**, Quantification of metastatic nodules present in livers on day 30 after bacterial therapy ($n=5$ per group, ****$P<0.0001$, unpaired two-tailed $t$-test). **c**, Kaplan–Meier survival curves for A20-tumor-bearing mice ($n=5$ per group, ***$P=0.0004$, log-rank (Mantel–Cox test)). **d**, Mice that had completely cleared A20 tumors were rechallenged with $10\times10^6$ A20 cells on day 90 after initial treatment. Naive mice received $5\times10^6$ A20 cells in each flank ($n=4$ mice per group). **e**, When A20 tumor volume reached 100–150 mm$^3$, mice received intratumoral (i.t.) injections of eSLC ($n=4$ tumors), eSLC–CD47nb bacterial lysate ($n=6$ tumors), rCD47nb (50 μg, $n=8$ tumors) or eSLC–CD47nb ($n=4$ tumors), or intraperitoneal (i.p.) injections of anti-CD47 monoclonal antibody (clone miap301, 400 μg, $n=6$ tumors) alone or in combination with intratumoral eSLC ($n=4$ tumors) for a total of four doses every 3–4 days. Tumor growth curves (****$P<0.0001$, ***$P=0.0002$, *$P=0.0162$, NS, not significant ($P>0.05$); two-way ANOVA with Tukey's multiple comparisons test). Tumor growth curves of tumors from individual mice are shown in Extended Data Fig. 3d. **f**, Tumor growth curves. BALB/c mice were implanted subcutaneously with $10^6$ 4T1-Luciferase mammary carcinoma cells. When tumors reached a volume of 200 mm$^3$, mice were randomized and received intratumoral injections of eSLC ($n=7$ tumors) or eSLC–CD47nb ($n=8$ tumors) every 3 days for a total of four doses (****$P<0.0001$, two-way ANOVA with Tukey's multiple comparisons test). Data are representative of two independent experimental replicates. Tumor growth curves of tumors from individual mice are shown in Extended Data Fig. 4b. **g**, In vivo images of lungs from mice bearing 4T1-Luciferase hind-flank tumors and quantification of number of 4T1-Luciferase metastatic foci in lungs of mice treated with eSLC or eSLC–CD47nb ($n=4$ mice per group, **$P=0.0036$, unpaired two-tailed $t$-test). **h**, Tumor growth curves of tumors from tumors from C57BL/6 mice subcutaneously injected with $5\times10^5$ B16-F10 melanoma cells in the hind flank. When tumors reached a volume of approximately 50–150 mm$^3$, mice were randomized and received intraperitoneal injections of miap301 (400 μg, $n=10$ tumors) or intratumoral injections of PBS ($n=8$ tumors), eSLC ($n=9$ tumors) or eSLC–CD47nb ($n=12$ tumors) every 3 days for a total of four doses (***$P=0.0002$, two-way ANOVA with Tukey's multiple comparisons test). Tumor growth curves of tumors from individual mice are shown in Extended Data Fig. 4c. **i**, BALB/c mice were injected with $5\times10^6$ A20 cells into both hind flanks. When tumor volume reached 100–200 mm$^3$, mice received intravenous injections of eSLC ($n=9$ tumors) or eSLC–CD47nb ($n=8$ tumors) or intraperitoneal injections of the anti-CD47 monoclonal antibody miap301 (400 μg, $n=10$ tumors) (****$P<0.0001$, two-way ANOVA with Tukey's multiple comparisons test). All data are mean ± s.e.m. Tumor growth curves of tumors from individual mice are shown in Extended Data Fig. 5a.

Recent studies have highlighted the importance of antigen-presenting cells and indicated that effector T cells are indispensable for anti-CD47-mediated clinical responses[30,31]. We reasoned that local inflammation induced by bacterial lysis coupled with localized blockade of CD47 on tumor cells would increase tumor cell phagocytosis and tumor antigen presentation, thereby enhancing

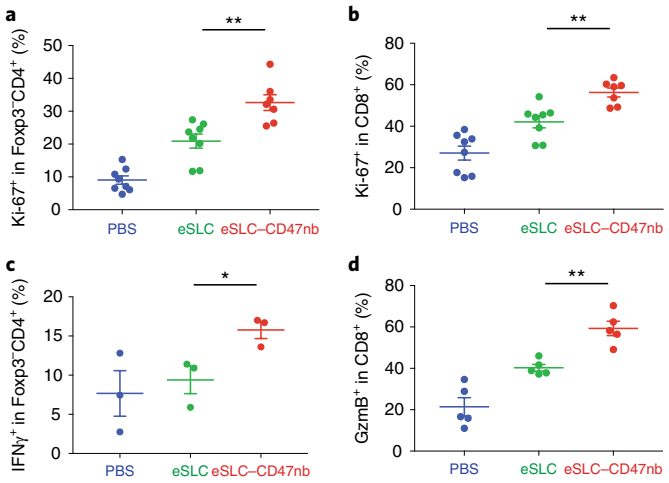


**Fig. 3 | Immunotherapeutic eSLC-CD47nb bacteria induce robust adaptive antitumor immune responses.** First, $5\times10^6$ A20 cells were implanted in the hind flanks of BALB/c mice. When tumors reached 100–150 $mm^3$ in volume (day 0), mice were treated with PBS, eSLC or eSLC-CD47nb on days 0, 4 and 7. Tumors were homogenized and tumor-infiltrating lymphocytes were isolated for flow cytometry analysis on day 8. **a**, Frequencies of isolated intratumoral Ki-67$^+$FOXP3$^-$CD4$^+$ and CD8$^+$ T cells from mice bearing tumors treated with PBS ($n=8$ tumors), eSLC ($n=8$ tumors) or eSLC-CD47nb ($n=7$ tumors) (**$P=0.0029$, unpaired two-tailed $t$-test). Data are pooled from two independent experimental replicates. **b**, Frequencies of isolated intratumoral Ki-67$^+$CD8$^+$ T cells from mice bearing tumors treated with PBS ($n=8$ tumors), eSLC ($n=8$ tumors) or eSLC-CD47nb ($n=7$ tumors) (**$P=0.0021$, unpaired two-tailed $t$-test). Data are pooled from two independent experimental replicates. **c**, Tumor-infiltrating lymphocytes were stimulated following ex vivo isolation with PMA and ionomycin in the presence of brefeldin A. Frequencies of intratumoral IFNγ$^+$FOXP3$^-$CD4$^+$ T cells following stimulation ($n=3$ tumors per group, *$P=0.0369$, unpaired two-tailed $t$-test). **d**, Percentages of intratumoral GzmB$^+$CD8$^+$ T cells ($n=5$ per group, **$P=0.0011$, unpaired two-tailed $t$-test). All data are shown as mean ± s.e.m.

the priming of antitumor T cells. Immunophenotyping of A20 tumors treated with eSLC–CD47nb revealed increased frequencies of MHC class II$^{hi}$CD11b$^+$F4/80$^+$ macrophages 3 days after commencing therapy (Extended Data Fig. 6a), suggesting an increase in the antigen-presentation ability of tumor macrophages at early time points. Additionally, on day 8, we observed a decline in SIRPα$^+$ macrophages within the tumor (Extended Data Fig. 6b). Previous studies have shown that lipopolysaccharide exposure leads to SIRPα downregulation on macrophages in vitro[38]. We hypothesized that combined release of lysis adjuvants and lack of SIRPα downstream signaling following CD47 blockade may lead to reduced surface expression of SIRPα on tumor-associated macrophages. Additionally, immunophenotyping of tumors treated with eSLC–CD47nb revealed increased proliferation of both FOXP3$^-$CD4$^+$ and CD8$^+$ T cells (Fig. 3a,b) in comparison to tumor-bearing mice treated with eSLC bacteria. Furthermore, tumor-infiltrating FOXP3$^-$CD4$^+$ T cells from eSLC–CD47nb-treated tumors produced significantly higher levels of IFNγ following ex vivo restimulation with phorbol myristate acetate (PMA) and ionomycin (Fig. 3c). Although we observed a trend towards higher IFNγ levels in CD8$^+$ T cells (Extended Data Fig. 6h), we observed markedly elevated levels of intratumoral granzyme B$^+$CD8$^+$ T cells (Fig. 3d) as well as other parameters of adaptive immune activation (Extended Data Fig. 6c–g). Additionally, these T cell responses appeared to be tumor-antigen-specific, as overnight in vitro co-culture of irradiated A20 cells with splenocytes derived from mice treated with eSLC–CD47nb led to robust secretion of IFNγ (Extended Data Fig. 7). Interestingly, mice treated with miap301 exhibited no elevated IFNγ response in comparison to those receiving eSLC–CD47nb. These data suggest that eSLC–CD47nb not only supports the activation and proliferation of intratumoral T cells, but also lead to the induction of systemic anti-A20 memory T cell responses.

Durable remission from cancer requires not only elimination of treated tumors, but also systemic antitumor immunity for the clearance of distant metastases. On the basis of our observation that eSLC–CD47nb enhances the effector function of tumor-infiltrating T cells within treated tumors, we examined whether eSLC–CD47nb could delay growth of untreated tumors. Mice injected with A20 tumors on both flanks were treated with eSLC–CD47nb in a unilateral fashion (Fig. 4a). Whereas control eSLC bacteria had no effect on the growth of untreated tumors, treatment of the primary tumor with eSLC–CD47nb substantially slowed the growth of untreated tumors on the opposing flank (Fig. 4b,c and Extended Data Fig. 8a). To further quantify this effect, we computed the mean growth rates (mm per day) of treated compared to untreated tumors by calculating the slopes in tumor volume trajectories for each mouse (Fig. 4d). These data indicated that tumors of eSLC–CD47nb-treated mice showed decreased growth rates for both treated and untreated tumors compared to controls. It has been shown that an intratumorally released nanobody does not lead to systemic CD47 blockade[33], providing evidence that the SLC-produced nanobody likely does not disseminate to the opposing, untreated tumor. However, we considered the possibility that eSLC–CD47nb bacteria injected into the primary tumor migrated through systemic circulation to seed the untreated lesion. We intratumorally injected a luminescent strain of SLC$^+$ *E. coli* (*E. coli* NisLux)[39] into a single tumor and performed in vivo imaging over 5 days. In comparison to a SLC$^-$ strain for which luminescence continuously increased over time, SLC$^+$ *E. coli* NisLux exhibited fluctuations in luminescence, indicating in vivo lysis behavior (Extended Data Fig. 8b,c). Importantly, the luminescent signal was limited to the injected lesion and the signal was undetectable in the untreated tumor or other organs, indicating that an adaptive immune response may be mediating this abscopal effect. In support of this hypothesis, flow cytometry analysis of lymphocytes isolated from untreated tumors of mice of which primary tumors were injected with eSLC–CD47nb showed increased frequencies of activated (Extended Data Fig. 9e) and proliferating (Fig. 4e) CD8$^+$ T cells as well as a trend towards increased frequencies of proliferating FOXP3$^-$CD4$^+$ T cells (Extended Data Fig. 9a). Additionally, we observed a significantly higher percentage of FOXP3$^-$CD4$^+$ and CD8$^+$ T cells producing IFNγ following ex vivo restimulation with PMA and ionomycin (Extended Data Fig. 9b,c). We directly assessed the reactivity of T cells in untreated tumors to an endogenous tumor antigen. Tumor-infiltrating lymphocytes were stimulated with an H-2Kd-restricted peptide (A20-Id, DYWGQGTEL), corresponding to the unique idiotype of the antibody expressed by A20 lymphoma cells, which has previously been shown to activate tumor-antigen-specific CD8$^+$ T cells[40]. Following ex vivo stimulation with A20-Id peptide, we observed a significantly higher frequency of IFNγ$^+$CD8$^+$ T cells in mice treated with eSLC–CD47nb in comparison to mice treated with eSLC or PBS (Fig. 4f). As further confirmation of the specificity of this assay, the frequency of IFNγ$^+$FOXP3$^-$CD4$^+$ T cells (Extended Data Fig. 9f) was unchanged—consistent with this peptide being MHC class I restricted. These data suggest that treatment with eSLC–CD47nb enhances tumor-antigen-specific CD8$^+$ T cell activity in the untreated tumor.

To further exclude the possibility of trafficking by bacteria, we assessed the biodistribution of SLC$^+$ *E. coli* at multiple time points after unilateral intratumoral injection. Plating of homogenized

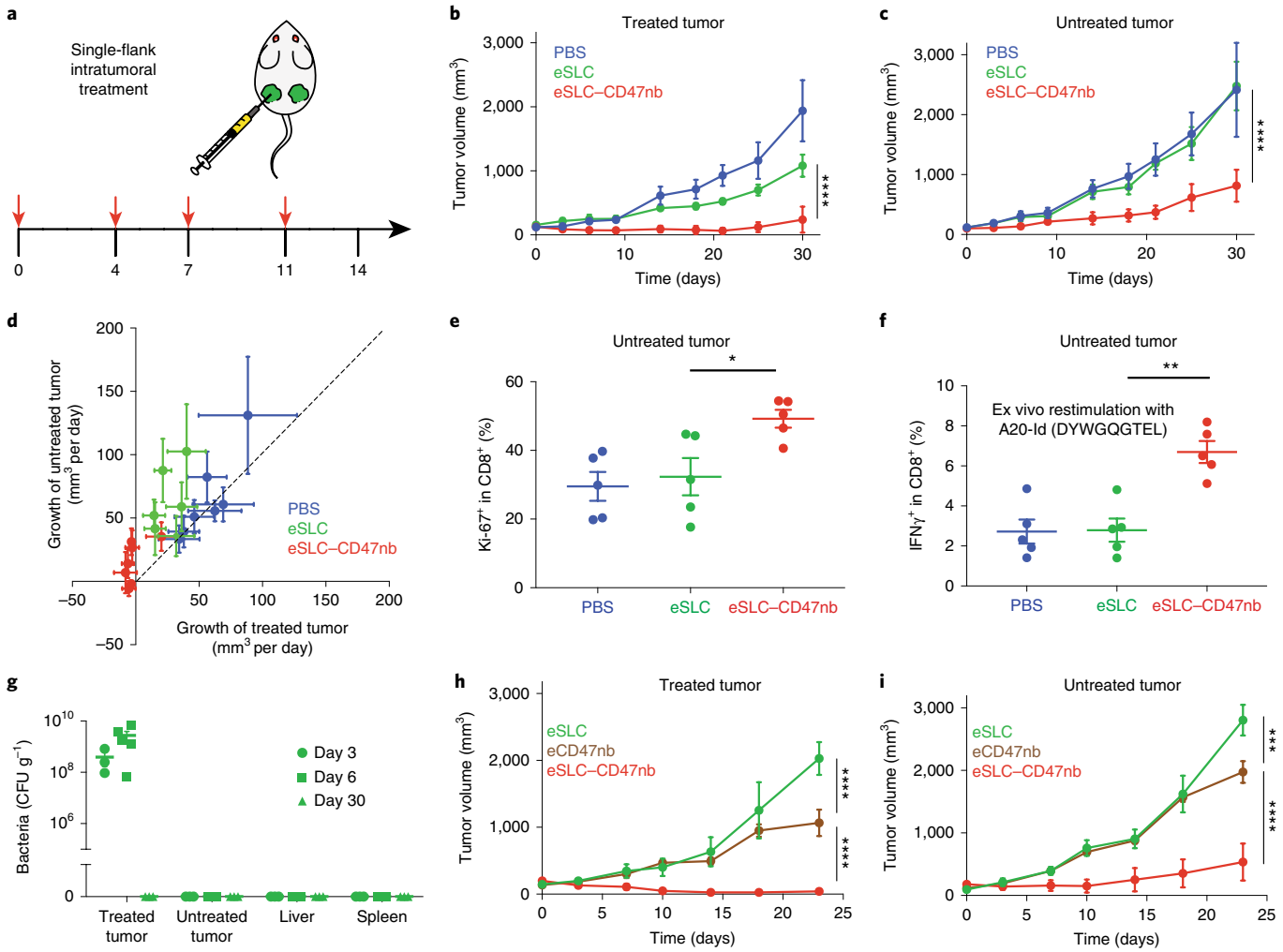


**Fig. 4 | Systemic adaptive immunity following bacterial therapy limits growth of untreated tumors. a**, Treatment schedule. BALB/c mice ($n=4$ mice per group) were implanted subcutaneously with $5\times10^6$ A20 cells on both hind flanks. When tumor volumes reached 100–150 mm$^3$, mice received intratumoral injections every 3–4 days of PBS, eSLC or eSLC-CD47 into a single tumor. **b**,**c**, Tumor growth curves of treated and untreated tumors (****$P<0.0001$, two-way ANOVA with Tukey's multiple comparisons test). Data are representative of three independent experimental replicates. Tumor growth curves of tumors from individual mice curves are shown in Extended Data Fig. 8a. **d**, Plot of tumor growth rate (mm$^3$ per day) of treated compared to untreated tumors for each mouse. Dotted line indicates slope = 1, points represent means, error bars represent s.e.m. **e**, Untreated tumors were isolated on day 8 after injection of bacteria into a single flank and analyzed by flow cytometry. Frequencies of intratumoral Ki-67$^+$CD8$^+$ T cells ($n=5$ per group, *$P=0.0229$, unpaired two-tailed $t$-test). Data are representative of two independent experimental replicates. **f**, Tumor-infiltrating lymphocytes were stimulated after ex vivo isolation with A20-Id peptide (DYWGQGTEL) in the presence of brefeldin A. Frequencies of intratumoral IFNγ$^+$CD8$^+$ T cells ($n=5$ per group, **$P=0.0012$, unpaired $t$-test). **g**, Biodistribution of SLC$^+$ *E. coli* on day 3 ($n=3$ mice), 6 ($n=5$ mice) and 30 ($n=3$ mice) after intratumoral injection of bacteria. Excised tumors, livers and spleens were homogenized and plated on LB-agar plates. Colonies were counted to determine CFU g$^{-1}$ of tissue. Limit of detection $10^3$ CFU g$^{-1}$. **h**,**i**, Tumor growth curves of treated and untreated A20 tumors following unilateral intratumoral injections of eSLC, eCD47nb or eSLC-CD47nb every 3–4 days for a total of four doses ($n=4$ per group, ***$P=0.001$, ****$P<0.0001$, two-way ANOVA with Tukey's multiple comparisons test). All data are mean ± s.e.m. Tumor growth curves of tumors from individual mice are shown in Extended Data Fig. 10a,b.

tumors and organs revealed that bacterial growth remained restricted to treated tumors and no bacteria could be cultured from untreated tumors or livers and spleens of treated mice above the limit of detection (approximately $1\times10^3$ colony-forming units (CFU); Fig. 4g). Furthermore, SLC-mediated CD47nb release appeared to be necessary for the induction of a potent abscopal effect. Although eCD47nb (a SLC$^-$ strain that constitutively produces CD47nb) administration slowed the growth of treated lesions in comparison to treatment with eSLC (Fig. 4h and Extended Data Fig. 10a), it exhibited a much weaker effect on untreated tumors in comparison to eSLC–CD47nb (Fig. 4i and Extended Data Fig. 10b). Taken together, these results demonstrate that the engineered quorum-lysis immunotherapeutic delivery system can generate potent, tumor-specific adaptive immune responses that operate systemically to clear distant tumor lesions.

This approach couples the inherently immunostimulatory nature of bacterial lysis products from programmable bacteria with potent nanobody-mediated blockade of an anti-phagocytic receptor. We observed enhanced proliferation and activation of tumor-infiltrating lymphocytes, leading to the induction of durable and systemic anti-tumor immunity. Our results suggest that localized, lysis-mediated release of the anti-CD47 nanobody confers multiple advantages over conventional systemic monoclonal antibody therapy—intratumoral delivery of a nanobody by

eSLC increases the local concentration of immunotherapy while simultaneously preventing systemic toxicity. Local treatment with eSLC–CD47nb promotes the induction of systemic antitumor immune responses that are not observed after treatment with an anti-CD47 monoclonal antibody. Finally, the ease of engineering bacteria to express additional immunotherapeutic nanobodies and/or cytokines, opens the possibility of evaluating combinations of several other immunotherapeutics that have exhibited systemic toxicity, but may be safe and effective when delivered intratumorally using eSLC. Our system allows for the delivery of immunotherapeutics in a spatiotemporally defined manner and permits delivery within diverse solid tumor settings. Moreover, owing to the observed abscopal effect, we provide a future strategy for treating metastatic lesions through the injection of accessible primary tumors.

## Online content

Any methods, additional references, Nature Research reporting summaries, source data, statements of code and data availability and associated accession codes are available at https://doi.org/10.1038/s41591-019-0498-z.

Received: 13 November 2018; Accepted: 24 May 2019;
Published online: 3 July 2019

## References

1. Fischbach, M. A., Bluestone, J. A. & Lim, W. A. Cell-based therapeutics: the next pillar of medicine. *Sci. Transl. Med.* **5**, 179ps177 (2013).
2. Weber, W. & Fussenegger, M. Emerging biomedical applications of synthetic biology. *Nat. Rev. Genet.* **13**, 21–35 (2012).
3. Lim, W. A. & June, C. H. The principles of engineering immune cells to treat cancer. *cell* **168**, 724–740 (2017).
4. Ruder, W. C., Lu, T. & Collins, J. J. Synthetic biology moving into the clinic. *Science* **333**, 1248–1252 (2011).
5. Chen, Y. Y. & Smolke, C. D. From DNA to targeted therapeutics: bringing synthetic biology to the clinic. *Sci. Transl. Med.* **3**, 106ps142 (2011).
6. Wu, M.-R., Jusiak, B. & Lu, T. K. Engineering advanced cancer therapies with synthetic biology. *Nat. Rev. Cancer* **19**, 187–195 (2019).
7. Chien, T., Doshi, A. & Danino, T. Advances in bacterial cancer therapies using synthetic biology. *Curr. Opin. Syst. Biol.* **5**, 1–8 (2017).
8. Din, M. O. et al. Synchronized cycles of bacterial lysis for in vivo delivery. *Nature* **536**, 81–85 (2016).
9. Pedrolli, D. B., Ribeiro, N. V., Squizato, P. N., de Jesus, V. N. & Cozetto, D. A. Engineering microbial living therapeutics: the synthetic biology toolbox. *Trends Biotechnol.* **37**, 100–115 (2019).
10. Zhou, S., Gravekamp, C., Bermudes, D. & Liu, K. Tumour-targeting bacteria engineered to fight cancer. *Nat. Rev. Cancer* **18**, 727–743 (2018).
11. Helmink, B. A., Khan, M. A. W., Hermann, A., Gopalakrishnan, V. & Wargo, J. A. The microbiome, cancer, and cancer therapy. *Nat. Med.* **25**, 377–388 (2019).
12. Sockolosky, J. T. et al. Durable antitumor responses to CD47 blockade require adaptive immune stimulation. *Proc. Natl Acad. Sci. USA* **113**, E2646–E2654 (2016).
13. Majeti, R. et al. CD47 is an adverse prognostic factor and therapeutic antibody target on human acute myeloid leukemia stem cells. *Cell* **138**, 286–299 (2009).
14. Willingham, S. B. et al. The CD47-signal regulatory protein alpha (SIRPa) interaction is a therapeutic target for human solid tumors. *Proc. Natl Acad. Sci. USA* **109**, 6662–6667 (2012).
15. Coley, W. B. Contribution to the knowledge of sarcoma. *Ann. Surg.* **14**, 199–220 (1891).
16. Berendt, M. J., North, R. J. & Kirstein, D. P. The immunological basis of endotoxin-induced tumor regression. Requirement for T-cell-mediated immunity. *J. Exp. Med.* **148**, 1550–1559 (1978).
17. Tsung, K. & Norton, J. A. Lessons from Coley's toxin. *Surg. Oncol.* **15**, 25–28 (2006).
18. Mellman, I., Coukos, G. & Dranoff, G. Cancer immunotherapy comes of age. *Nature* **480**, 480–489 (2011).
19. Jiang, S. N. et al. Inhibition of tumor growth and metastasis by a combination of *Escherichia coli*-mediated cytolytic therapy and radiotherapy. *Mol. Ther.* **18**, 635–642 (2010).
20. Malmgren, R. A. & Flanigan, C. C. Localization of the vegetative form of *Clostridium tetani* in mouse tumors following intravenous spore administration. *Cancer Res.* **15**, 473–478 (1955).
21. Brown, J. M. & Wilson, W. R. Exploiting tumour hypoxia in cancer treatment. *Nat. Rev. Cancer* **4**, 437–447 (2004).
22. Forbes, N. S. Engineering the perfect (bacterial) cancer therapy. *Nat. Rev. Cancer* **10**, 785–794 (2010).
23. Zheng, J. H. et al. Two-step enhanced cancer immunotherapy with engineered *Salmonella typhimurium* secreting heterologous flagellin. *Sci. Transl. Med.* **9**, eaak9537 (2017).
24. Gardner, T. S., Cantor, C. R. & Collins, J. J. Construction of a genetic toggle switch in *Escherichia coli*. *Nature* **403**, 339–342 (2000).
25. Basu, S., Gerchman, Y., Collins, C. H., Arnold, F. H. & Weiss, R. A synthetic multicellular system for programmed pattern formation. *Nature* **434**, 1130–1134 (2005).
26. Friedland, A. E. et al. Synthetic gene networks that count. *Science* **324**, 1199–1202 (2009).
27. Danino, T., Mondragon-Palomino, O., Tsimring, L. & Hasty, J. A synchronized quorum of genetic clocks. *Nature* **463**, 326–330 (2010).
28. Elowitz, M. B. & Leibler, S. A synthetic oscillatory network of transcriptional regulators. *Nature* **403**, 335–338 (2000).
29. Jaiswal, S. et al. CD47 is upregulated on circulating hematopoietic stem cells and leukemia cells to avoid phagocytosis. *Cell* **138**, 271–285 (2009).
30. Liu, X. et al. CD47 blockade triggers T cell-mediated destruction of immunogenic tumors. *Nat. Med.* **21**, 1209–1215 (2015).
31. Kauder, S. E. et al. ALX148 blocks CD47 and enhances innate and adaptive antitumor immunity with a favorable safety profile. *PLoS ONE* **13**, e0201832 (2018).
32. Liu, X. et al. Dual targeting of innate and adaptive checkpoints on tumor cells limits immune evasion. *Cell Rep.* **24**, 2101–2111 (2018).
33. Ingram, J. R. et al. Localized CD47 blockade enhances immunotherapy for murine melanoma. *Proc. Natl Acad. Sci. USA* **114**, 10184–10189 (2017).
34. Huang, Y., Ma, Y., Gao, P. & Yao, Z. Targeting CD47: the achievements and concerns of current studies on cancer immunotherapy. *J. Thorac. Dis.* **9**, E168–E174 (2017).
35. Advani, R. et al. CD47 blockade by Hu5F9-G4 and rituximab in non-Hodgkin's lymphoma. *N. Engl. J. Med.* **379**, 1711–1721 (2018).
36. Veillette, A. & Chen, J. SIRPα–CD47 immune checkpoint blockade in anticancer therapy. *Trends Immunol.* **39**, 173–184 (2018).
37. Skinner, S. O., Sepulveda, L. A., Xu, H. & Golding, I. Measuring mRNA copy number in individual *Escherichia coli* cells using single-molecule fluorescent in situ hybridization. *Nat. Protoc.* **8**, 1100–1113 (2013).
38. Kong, X. N. et al. LPS-induced down-regulation of signal regulatory protein α contributes to innate immune activation in macrophages. *J. Exp. Med.* **204**, 2719–2731 (2007).
39. Danino, T. et al. Programmable probiotics for detection of cancer in urine. *Sci. Transl. Med.* **7**, 289ra84 (2015).
40. Armstrong, A. C. et al. Immunization with a recombinant adenovirus encoding a lymphoma idiotype: induction of tumor-protective immunity and identification of an idiotype-specific T cell epitope. *J. Immunol.* **168**, 3983–3991 (2002).

## Acknowledgements

This work was supported by the NIH Pathway to Independence Award (R00CA197649–02) (to T.D.), DoD Idea Development Award (LC160314) (to T.D.), DoD Era of Hope Scholar Award (BC160541) (to T.D.), NIH R01GM069811 (to T.D.), NIH K22AI127847 (to N.A.), Searle Scholars Program SSP-2017-2179 (to N.A.), Bonnie J. Addario Lung Cancer Foundation Young Investigators Team Award (to N.A. and T.D.) and the Roy and Diana Vagelos Precision Medicine Pilot Grant (to N.A. and T.D.). Research reported in this publication was performed in the Columbia University Department of Microbiology and Immunology Flow Cytometry Core facility. The content is solely the responsibility of the authors and does not necessarily represent the official views of the National Institutes of Health. We thank K. T. Fortson and O. Velasquez for technical assistance with flow cytometry experiments and in vivo tumor experiments, respectively; M. O. Din for input pertaining to SLC characterization experiments; and V. Yeong and members of the Obermeyer group for assistance with affinity chromatography and protein purification. We thank R. L. Vincent, T. M. Savage, K. A. Kaiser and L. F. Loffredo for critical review of the manuscript.

## Author contributions

S. Chowdhury, N.A. and T.D. conceived and designed the study. S. Chowdhury, S. Castro, C.C. and T.E.H. performed in vivo experiments. S. Chowdhury performed in vitro characterization of eSLC–CD47nb and conducted immunophenotyping experiments. S. Chowdhury, N.A. and T.D. analyzed data and wrote the manuscript with input from all other authors.

## Competing interests

S. Chowdhury, N.A. and T.D. have filed a provisional patent application with the US Patent and Trademark Office (US Patent Application No. 62/747,826) related to this work. T.D. and N.A. have a financial interest in GenCirq, Inc.

## Additional information

**Extended data** is available for this paper at https://doi.org/10.1038/s41591-019-0498-z.

**Supplementary information** is available for this paper at https://doi.org/10.1038/s41591-019-0498-z.



**Correspondence and requests for materials** should be addressed to T.D. and N.A.



**Peer review information:** Saheli Sadanand and Joao Monteiro were the primary editors on this article and managed its editorial process and peer review in collaboration with the rest of the editorial team.

## Methods

**Strains and plasmids.** Plasmids were constructed using Gibson assembly or standard restriction enzyme-mediated cloning methods. The pSC01 SLC plasmid was constructed by first amplifying a region that contained the constitutively expressed *luxR* gene and phage lysis gene, ϕX174E under the control of the *luxI* promoter from a pZA35E plasmid[8]. Next, this region was cloned into a pTD103-luxI plasmid[27] using the AvrII site. The pSC02 therapeutic plasmid was constructed by cloning a gBlock (IDT) encoding a *tac* promoter and an *E. coli* codon-optimized sequence for the A4 anti-CD47 nanobody[12] with an C-terminal HA tag into the multiple cloning site of a pAH162 plasmid[41]. Additionally, two stabilizing elements, the hok/sok system[42] and alp7 partitioning system[43] were introduced into pSC02 to minimize plasmid loss in vivo. pSC01 and pSC02 were transformed into chemically competent *E. coli* Pir1$^+$ (Invitrogen). eSLC strains were grown in LB medium with 50 μg ml$^{-1}$ kanamycin (pSC01) and 100 μg ml$^{-1}$ tetracycline (pSC02) along with 0.2% glucose at 37 °C for under 12 h in a shaking incubator. Glucose was added to reduce expression from the Lux promoter and prevent lysis in vitro. The pSC04 protein expression plasmid was constructed by cloning a gBlock (IDT) that encodes an *E. coli* codon-optimized sequence for the A4 anti-CD47 nanobody[12] with a C-terminal 6×His tag into the multiple cloning site of an 1-thio-D-galactopyranoside (IPTG)-inducible pET vector containing ampicillin resistance (100 μg ml$^{-1}$). pSC04 was transformed into NiCo21(DE3) *E. coli* (NEB).

**Characterization of the SLC.** To validate SLC function, SLC$^+$ and SLC$^-$ *E. coli* were inoculated in LB medium, which contained the appropriate antibiotics, and diluted 1:10. Samples were grown at 37 °C in a round-bottom 96-well plate in a shaking Tecan plate reader. The $OD_{600}$ was recorded every 10 min for 20 h. Agar pads were prepared according to previous protocols[37]. SLC$^+$ and SLC$^-$ *E. coli* were inoculated in LB medium, which contained the appropriate antibiotics, and grown to mid-log phase. They were diluted 1:100 and grown under agar pads at 37 °C and imaged using a Nikon Ti-E microscope equipped with an Okolab stage top incubator.

**Bacterial nanobody characterization.** For purification of rCD47nb, pSC04-containing NiCo21(DE3) *E. coli* were grown at 37 °C to an $OD_{600}$ of approximately 0.8 and induced with 1 mM IPTG for 20 h at 30 °C. Cells were centrifuged at 4,000 r.p.m. for 10 min. After resuspension in lysis buffer (50 mM $NaH_2PO_4$, 300 mM NaCl, pH 8.0) and sonication, lysates were spun at 10,000 r.p.m. for 30 min at 4 °C. The supernatant was loaded on to Ni-NTA (Qiagen) resin and washed in wash buffer (35 mM imidazole), followed by elution in 250 mM imidazole. The elutions were then dialyzed in PBS using regenerated cellulose dialysis tubing (3,500 Da MWCO) and the solution was filtered through a 0.2-μm filter to remove any residual debris and stored at −80 °C.

Overnight cultures of *E. coli* containing pSC01 and pSC02 were grown in appropriate antibiotics and 0.2% glucose. A 1:100 dilution into LB with antibiotics was made the following day and bacteria were grown in a shaking incubator at 37 °C. $OD_{600}$ was measured every 30 min until the $OD_{600}$ of lysing strains began to fall, indicating lysis. At this point, OD-normalized bacteria were spun down at 3,800 r.p.m. and supernatants were filtered through a 0.2 μm filter. Cell pellets were mechanically lysed by 3–4 freeze-thaw cycles. Supernatants and lysates were separated by SDS-PAGE followed by immunoblotting with rat anti-HA (Sigma) antibody to evaluate the presence of rCD47nb in culture fractions. To verify binding of bacterially produced nanobody to CD47 on tumor cells, serial dilutions of bacterial supernatants from SLC bacteria with or without pSC02 or rCD47nb were co-incubated with FITC-labeled anti-CD47 antibody in the presence of A20 tumor cells for 1 h and FITC fluorescence was measured by flow cytometry.

**In vitro phagocytosis.** Overnight cultures of *E. coli* containing pSC01 and pSC02 were grown in appropriate antibiotics and 0.2% glucose. A 1:100 dilution into LB with antibiotics was made the following day and bacteria were grown to mid-log phase in a shaking incubator at 37 °C. Bacteria were pelleted at 3,800 r.p.m. and lysed by sonication. To obtain eSLC and eSLC–CD47nb lysates, sonicates were spun at 10,000 r.p.m. for 5 min and supernatants were filtered through a 0.2-μm filter to remove any residual debris. Collected BMDMs were detached and seeded onto a transparent 96-well tissue culture plate at $5\times10^4$ cells per well. A20 tumor cells were incubated for 10 min with 5 μM Vybrant DiI solution (Invitrogen). Labeled A20 cells were pretreated with serial dilutions of bacterial lysates (eSLC or eSLC–CD47nb) or with anti-CD47 monoclonal antibody, isotype antibody or PBS. After 3.5 h co-incubation of labeled, pretreated A20 cells and BMDMs, residual A20 cells were washed and BMDMs were stained with NucBlue. Multiple random fields were imaged for each replicate using a Nikon Ti-E microscope. The ratio of DiI$^+$ BMDMs to total NucBlue$^+$ BMDMs was counted for each field to score phagocytosis.

**Animal models.** All animal experiments were approved by the Institutional Animal Care and Use Committee (Columbia University, protocols AC-AAAN8002 and AC-AAAZ4470). The protocol requires animals to be euthanized when the tumor burden reaches 2 cm in diameter or after recommendation by the veterinary staff. Mice were blindly randomized into various groups. Animal experiments were performed on 4–8-week-old female BALB/c mice or C57BL/6 mice (Taconic Biosciences) with bilateral subcutaneous hind-flank tumors from A20 mouse lymphoma cells (ATCC), 4T1-luciferase mammary carcinoma cells (ATCC, luciferized by stable plasmid transfection) or B16-F10 melanoma cells. Cells were injected subcutaneously at a volume of 100 μl per flank, with each implant consisting of $5\times10^6$ cells (BALB/c, A20), $10^6$ cells (BALBc, 4T1) or $5\times10^5$ (C57BL/6, B16-F10). Tumors were grown to an average volume of approximately 100–200 mm$^3$ before treatment with bacterial strains. Tumor volume was calculated by measuring the length and width of each tumor using calipers, where $V = \text{length}\times\text{width}^2\times0.5$ as previously calculated[30]. For all tumor growth experiments, a minimum of four mice per group were used. The growth in mm per day was computed by taking the difference between tumor volumes at adjacent time points for a particular animal. Values were computed as the mean ± s.e.m.

**Bacterial administration for in vivo experiments.** Bacterial strains were grown overnight in LB medium, which contained the appropriate antibiotics and 0.2% glucose. A 1:100 dilution into medium with antibiotics was started the day of injection and grown to an $OD_{600}$ of approximately 0.1. Bacteria were spun down and washed three times with sterile PBS before injection into mice. Intratumoral injections of bacteria were performed at a concentration of $5\times10^8$ CFU ml$^{-1}$ in PBS with a total volume of 20–40 μl injected per tumor. Tail-vein (intravenous) injections of bacteria were performed at a concentration of $5\times10^7$ CFU ml$^{-1}$ in PBS with a total volume of 100 μl injected per mouse.

**Biodistribution and in vivo bacterial dynamics.** Following treatment with $10^7$ SLC$^+$ *E. coli*, tumors, spleen and liver were weighed and homogenized using a gentleMACS tissue dissociator (Miltenyi Biotec; C-tubes). Homogenates were serially diluted and plated on LB–agar plates at 37 °C overnight. Colonies were counted (limit-of-detection $10^3$ CFU g$^{-1}$) and computed as CFU g$^{-1}$ of tissue. To determine in vivo dynamics of SLC$^+$ and SLC$^-$ *E. coli*, $10^7$ SLC$^+$ or SLC$^-$ *E. coli* NisLux (genomic expression of luxCDABE cassette) were injected unilaterally into hind-flank tumors. The luminescent signal was measured at multiple time points over 4 days with an in vivo imaging system after injection of bacteria to follow dynamics.

**Flow cytometry.** Tumors were extracted for immunophenotyping on day 3 or day 8 after the initiation of bacterial therapy. Myeloid and lymphoid subsets were isolated from tumor tissue by mechanical homogenization of tumor tissue followed by digestion with collagenase A (1 mg ml$^{-1}$; Roche) and DNase I (0.5 μg ml$^{-1}$; Roche) in isolation buffer (RPMI 1640 supplemented with 5% FBS, 1% L-glutamine, 1% penicillin–streptomycin and 10 mM HEPES) for 1 h at 37 °C. Cells were filtered through 100-μm cell strainers, washed in isolation buffer and stained. Dead cells were excluded by staining with Ghost Dye cell viability reagent. Extracellular antibodies included anti-B220 (BD), anti-CD4 (Tonbo), anti-CD8 (eBioscience), anti-NKp46 (BD), anti-Gr-1 (Tonbo) anti-CD11b (BD), anti-F4/80 (eBioscience), anti-SIRPα (BioLegend) and anti-MHC class II (Tonbo) antibodies. To measure the production of cytokines by T cells, cells were stimulated for 2 h with PMA (50 ng ml$^{-1}$; Sigma-Aldrich) and ionomycin (1 nM; Calbiochem) in the presence of GolgiPlug (brefeldin A). To measure tumor-antigen-specific production of cytokines by T cells, cells were stimulated for 5 h with A20-Id (DYWGQGTEL) peptide (GenScript) for 5 h in the presence of GlogiPlug (brefeldin A). Following extracellular staining with the aforementioned antibodies, intracellular staining was performed using anti-CD3 (Tonbo), anti-TCRβ (BD), anti-CTLA4 (eBioscience), anti-FOXP3 (eBioscience), anti-Ki-67 (Thermo), anti-granzyme-B (Biolegend) antibodies and cytokines (anti-IL-17 (eBioscience), anti-TNF (eBioscience), anti-IFNγ (Tonbo) antibodies). Cells were fixed using the FOXP3/transcription factor staining buffer set (Tonbo) as per the manufacturer's protocol. Samples were analyzed using a BD LSRFortessa cell analyzer.

**Statistical analysis.** Statistical tests were calculated in GraphPad Prism v.7.0 and v.8.0. The details of the statistical tests carried out are indicated in the respective figure legends. Where data were approximately normally distributed, values were compared using either a Student's *t*-test or one-way ANOVA for single variables, or using a two-way ANOVA for two variables with Tukey's correction for multiple comparisons. For Kaplan–Meier survival experiments, we performed a log-rank (Mantel–Cox) test. Mice were randomized into different groups before experiments.

**Reporting Summary.** Further information on research design is available in the Nature Research Reporting Summary linked to this article.

## Data availability

All requests for raw and analyzed data and materials will be promptly reviewed by Columbia Technology Ventures to verify whether the request is subject to any intellectual property or confidentiality obligations. Any data and materials that can be shared will be released through a material transfer agreement.

## References

41. Haldimann, A. & Wanner, B. L. Conditional-replication, integration, excision, and retrieval plasmid-host systems for gene structure-function studies of bacteria. *J. Bacteriol.* **183**, 6384–6393 (2001).
42. Gerdes, K. et al. Mechanism of postsegregational killing by the hok gene product of the parB system of plasmid R1 and its homology with the relF gene product of the *E. coli* relB operon. *EMBO J.* **5**, 2023–2029 (1986).
43. Derman, A. I. et al. Alp7R regulates expression of the actin-like protein Alp7A in *Bacillus subtilis*. *J. Bacteriol.* **194**, 2715–2724 (2012).

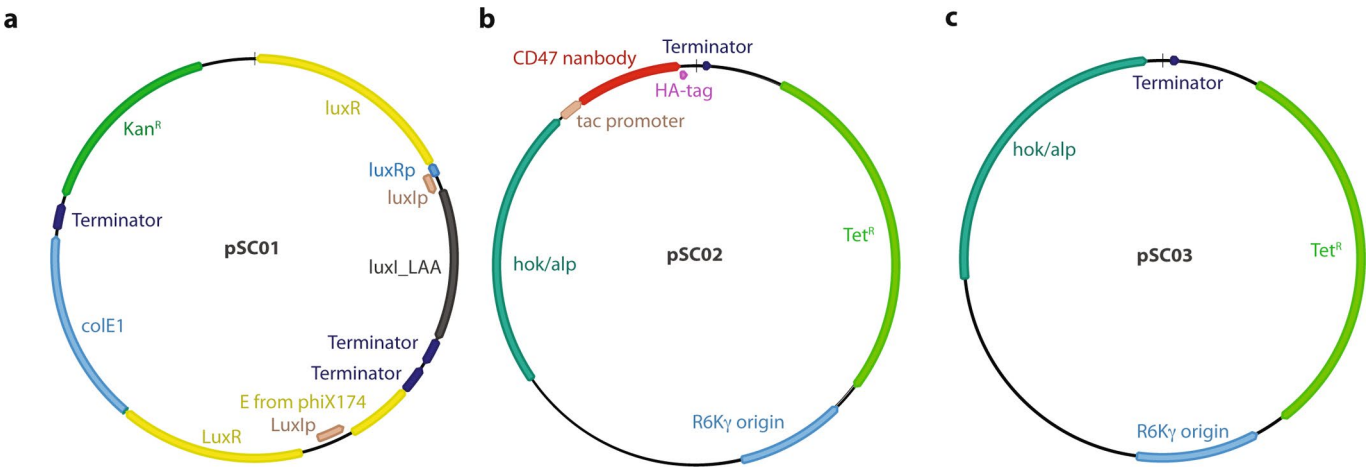


**Extended Data Fig. 1 | Map of plasmids used in this study. a**, pSC01, single plasmid with synchronized lysis circuit. **b**, pSC02, stabilized plasmid that drives constitutive expression of HA-tagged anti-CD47 nanobody. **c**, pSC03, empty vector control.

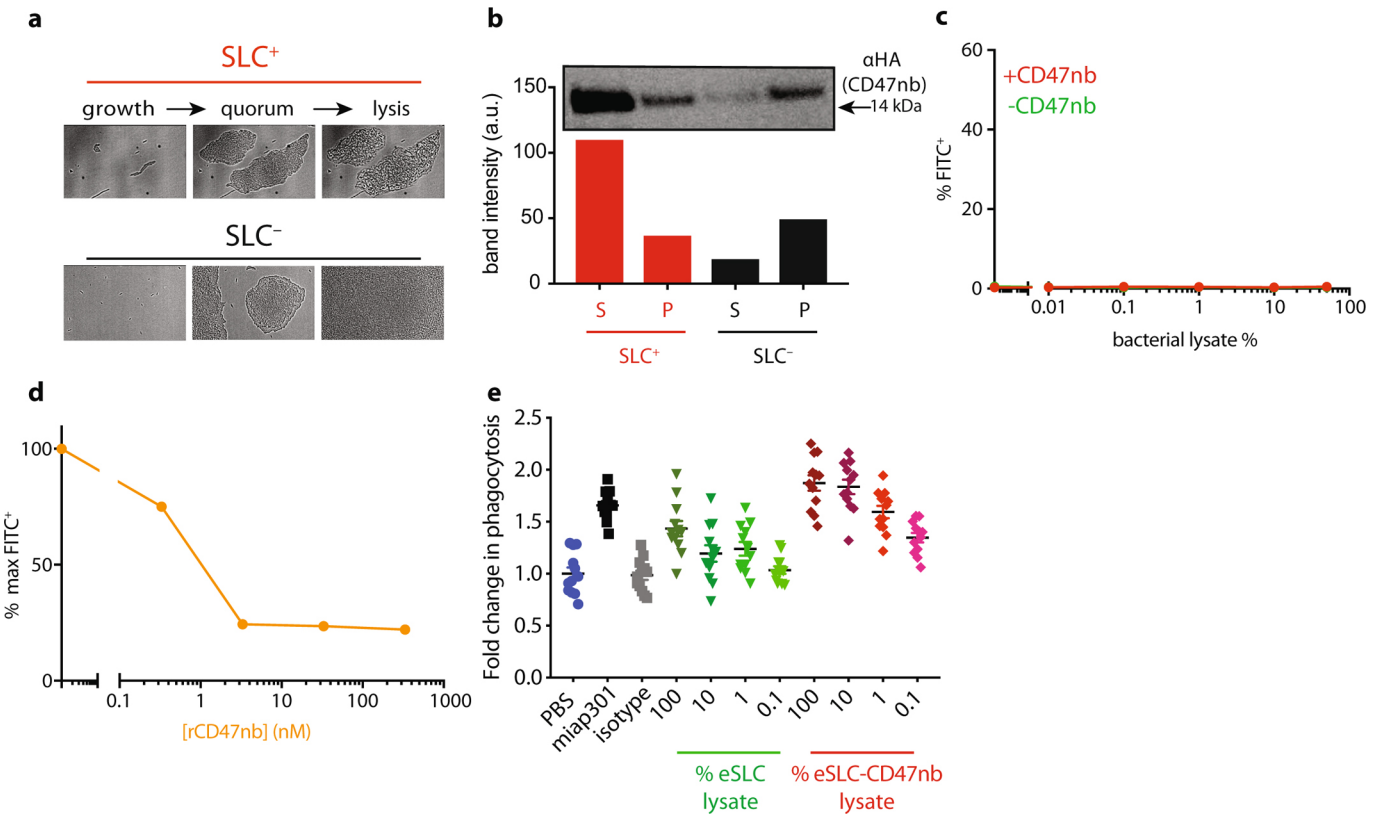


**Extended Data Fig. 2 | *E. coli* that are capable of synchronized lysis produce functional anti-CD47 nanobodies. a**, Bacterial growth dynamics over time in agar-pad microscopy experiments. **b**, Immunoblot of bacterial culture supernatants (S) and cell pellets (P) in strains with and without SLC designed to constitutively produce the HA-tagged CD47 nanobody. a.u., arbitrary units. Data are representative of three independent experimental replicates. The immunoblot has been cropped to show relevant bands; a molecular weight marker is indicated on the right (in kDa). The uncropped blot is available as Source Data. **c**, A20 cells were co-incubated with a fixed concentration of FITC-conjugated isotype control (IgG2a–FITC) antibody along with increasing concentrations of bacterial lysates of bacteria that constitutively expressed CD47nb or empty vector. Data are representative of two independent experimental replicates. **d**, A20 cells were co-incubated with a fixed concentration of FITC-conjugated anti-CD47 (miap301) antibody along with serial dilutions of recombinant 6×His-tagged rCD47nb. Data are representative of two independent experimental replicates. **e**, In vitro phagocytosis by BMDMs of DiI-labeled A20 cells pretreated with PBS, miap301 or IgG2a isotype control, or with serial dilutions of eSLC or eSLC–CD47nb lysates in PBS. Data are mean ± s.e.m., $n = 4$ fields of view from three technical replicates.

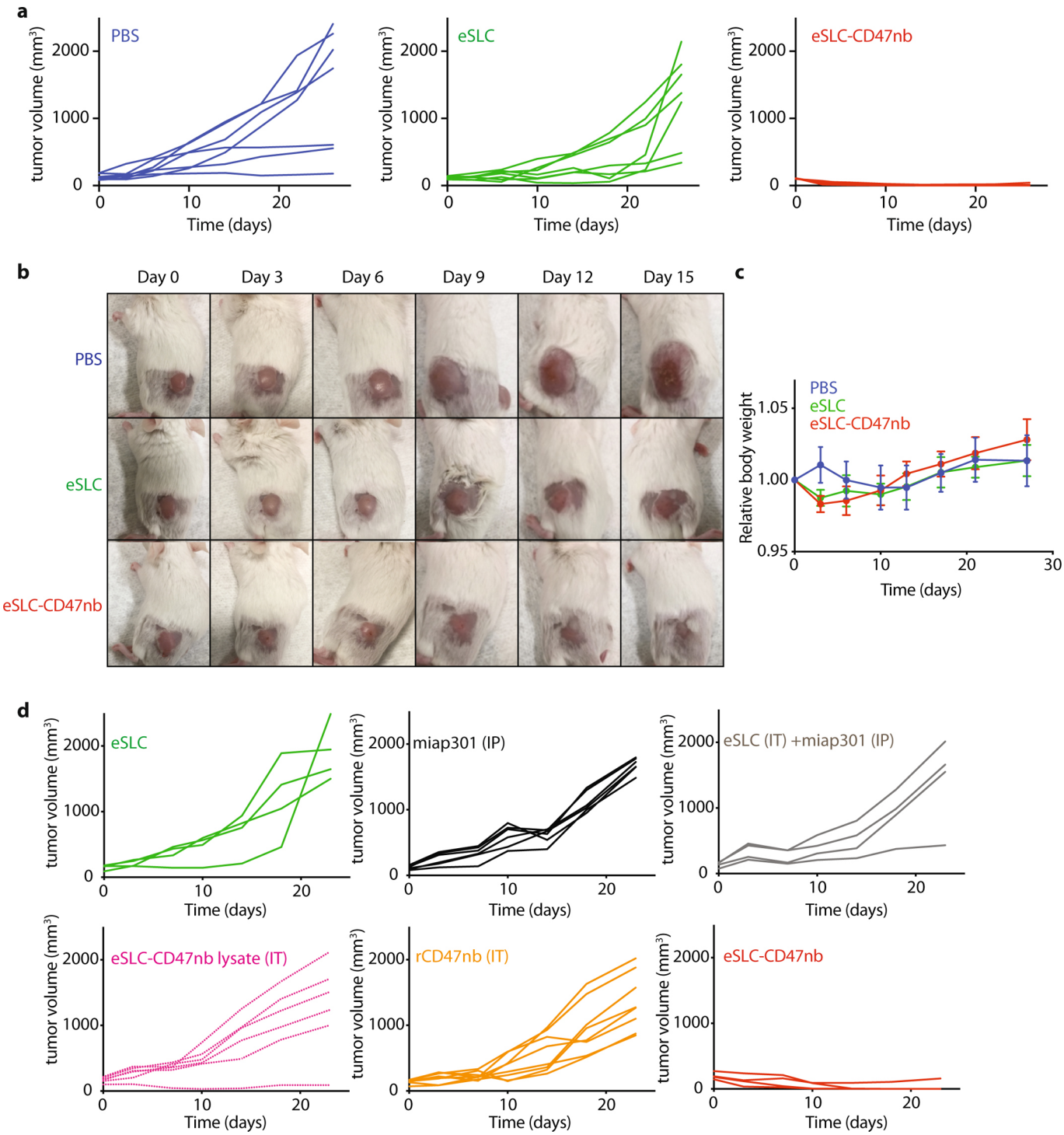


**Extended Data Fig. 3 | Individual kinetics of intratumoral bacterial immunotherapy. a**, Individual tumor growth trajectories ($n = 7$ mice per group); related to data shown in Fig. 2a. **b**, Representative images of subcutaneous A20-tumor-bearing BALB/c mice treated with PBS, eSLC or eSLC-CD47nb. **c**, Relative body weight of A20-tumor-bearing BALB/c mice over time ($n = 7$ mice per group; $P > 0.05$, two-way ANOVA with Tukey's multiple comparisons test). Data are mean ± s.e.m. **d**, Individual tumor growth trajectories after treatment with eSLC (intratumoral injection (IT)), miap301 (intraperitoneal injection (IP)), eSLC (intratumoral injection) and miap301 (intraperitoneal injection), eSLC-CD47nb lysate, rCD47nb (intratumoral injection) or eSLC-CD47nb (intratumoral injection); related to data shown in Fig. 2e.

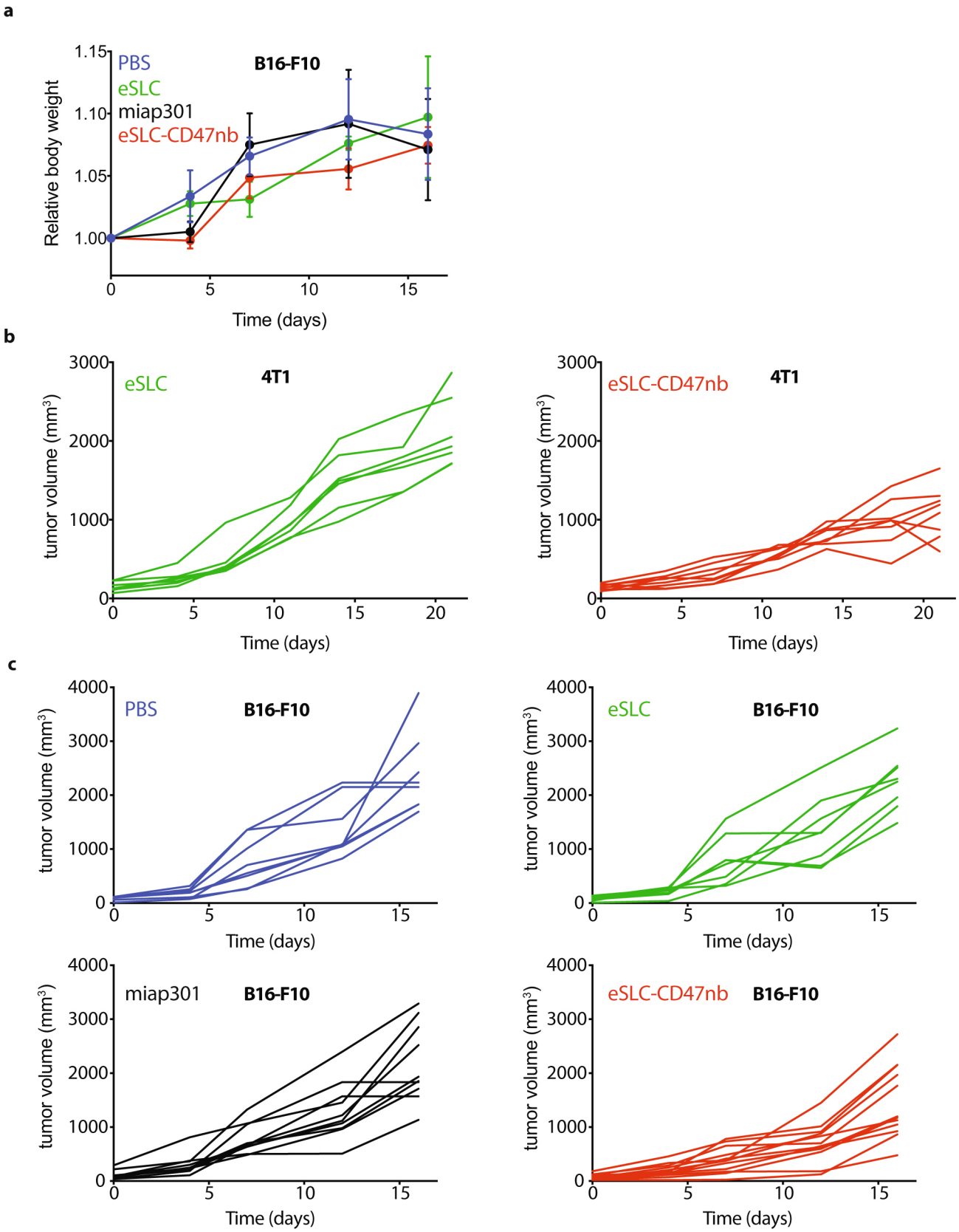


**Extended Data Fig. 4 | Immunotherapeutic bacteria limit tumor growth in syngeneic mouse models of melanoma and triple-negative breast cancer.** **a**, Relative body weight of B16-F10-bearing C57BL/6 mice over time. Mice were treated with PBS ($n=4$ mice), eSLC ($n=5$ mice), miap301 ($n=5$ mice) or eSLC-CD47nb ($n=6$ mice) ($P<0.05$, two-way ANOVA with Tukey's multiple comparisons test). Data are mean ± s.e.m. **b**, Individual tumor growth trajectories of subcutaneous 4T1 tumors after intratumoral injection of eSLC ($n=7$ tumors) or eSLC-CD47nb ($n=8$ tumors); related to data shown in Fig. 2f. **c**, Individual tumor growth trajectories of subcutaneous B16-F10 melanoma after intraperitoneal injection of miap301 or intratumoral injection of PBS, eSLC or eSLC-CD47nb; related to data shown in Fig. 2h.

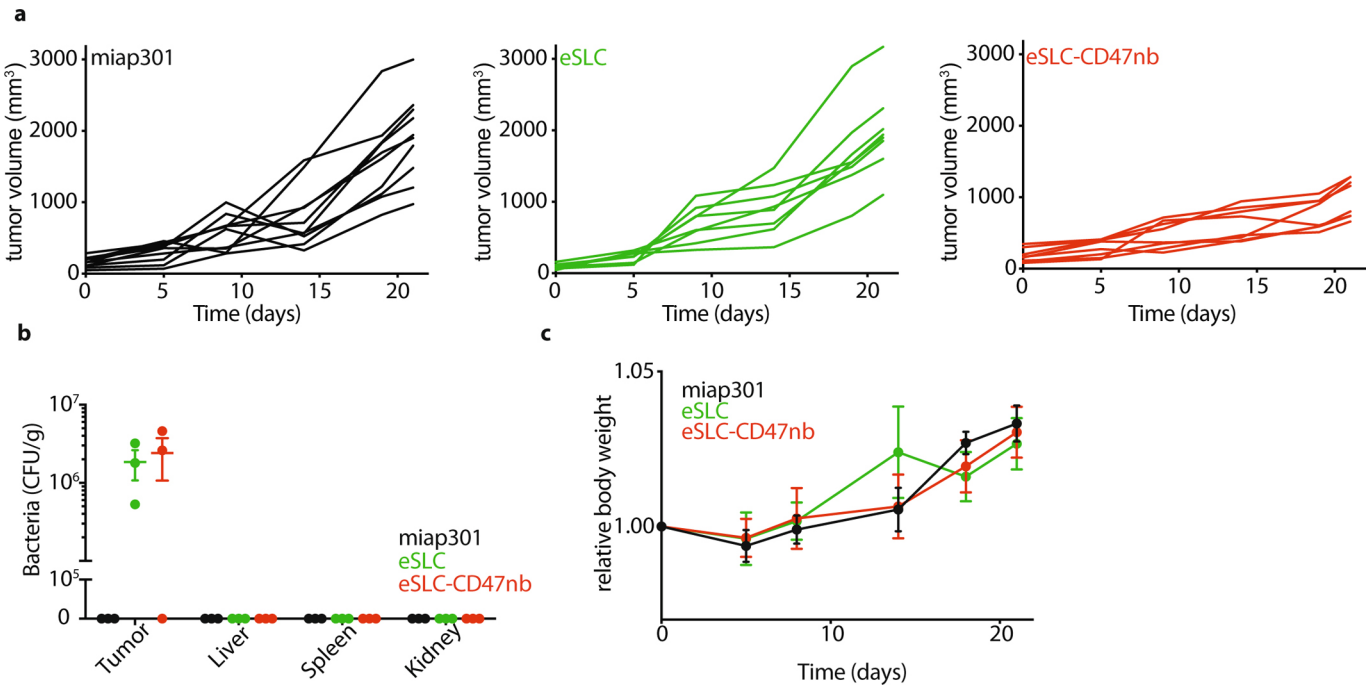


**Extended Data Fig. 5 | Intravenous bacterial immunotherapy limits tumor growth in mice in a subcutaneous A20 lymphoma model. a**, Individual tumor growth trajectories of subcutaneous A20 tumors after intraperitoneal injection of miap301 ($n=10$ tumors) or intravenous injection of eSLC ($n=9$ tumors) or eSLC-CD47nb ($n=10$ tumors); related to data shown in Fig. 2i. **b**, Biodistribution of eSLC-CD47nb *E. coli* on day 8 after the final intravenous bacterial treatment. Excised tumors, livers, spleens and kidneys were homogenized, serially diluted and plated onto LB-agar plates. Colonies were counted to determine the CFU $g^{-1}$ of tissue ($n=3$ per group). Data are mean ± s.e.m. **c**, Relative body weight of A20-tumor-bearing BALB/c mice that received intravenous injections of bacteria (eSLC, $n=5$ mice; eSLC-CD47nb, $n=4$ mice) or intraperitoneal injections of miap301 ($n=5$ mice) ($P>0.05$, two-way ANOVA with Tukey's multiple comparisons test). Data are mean ± s.e.m.

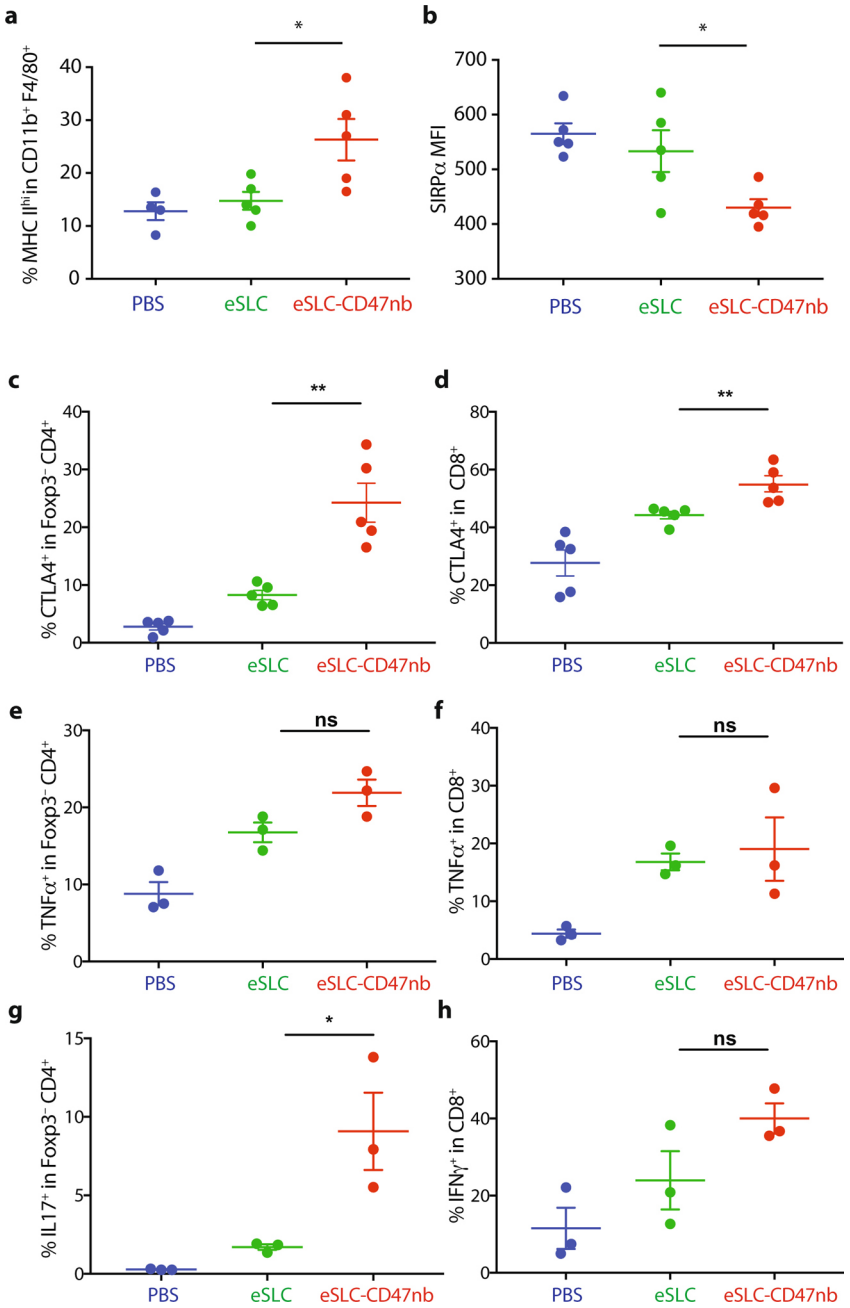


**Extended Data Fig. 6 | Immunophenotyping of tumor-infiltrating myeloid and lymphoid cell subsets after intratumoral injection of bacteria.** First, $5\times10^6$ A20 cells were subcutaneously implanted into the hind flanks of BALB/c mice. Subsequently, when tumors reached 100–150 $mm^3$ in volume (day 0), mice were treated with PBS, eSLC or eSLC-CD47nb on days 0, 4 and 7. On day 3 or day 8, tumors were homogenized and tumor-infiltrating myeloid and lymphoid cell subsets were isolated for flow cytometry analysis. **a**, Frequency of isolated MHC class II$^{hi}$CD11b$^+$F4/80$^+$ macrophages on day 3 after treatment ($n=5$ tumors per group, $^*P=0.0271$, unpaired two-tailed $t$-test). **b**, Mean fluorescence intensity (MFI) of SIRPα staining within the CD11b$^+$F4/80$^+$ subset on day 8 after treatment ($n=5$ tumors per group, $^*P=0.0209$, unpaired two-tailed $t$-test). **c**,**d**, Frequencies of CTLA4$^+$ cells within the FOXP3$^-$CD4$^+$ T cell population (**c**; $n=5$ tumors per group, $^{**}P=0.0018$, unpaired two-tailed $t$-test) and CD8$^+$ T cell population (**d**; $n=5$ tumors per group, $^{**}P=0.0098$, unpaired two-tailed $t$-test). **e**,**f**, Frequencies of TNF$^+$ cells within FOXP3$^-$CD4$^+$ T cell (**e**) and CD8$^+$ T cell (**f**) populations following ex vivo stimulation (ns, not significant ($P>0.05$), $n=3$ tumors per group, unpaired two-tailed $t$-test). **g**, Frequency of IL-17$^+$ cells within the FOXP3$^-$CD4$^+$ T cell population following ex vivo stimulation ($^*P=0.0402$, $n=3$ tumors per group, unpaired two-tailed $t$-test). **h**, Frequency of IFNγ$^+$ cells within the CD8$^+$ T cell population following ex vivo stimulation ($n=3$ tumors per group, $P>0.05$, unpaired two-tailed $t$-test). All data are mean ± s.e.m.

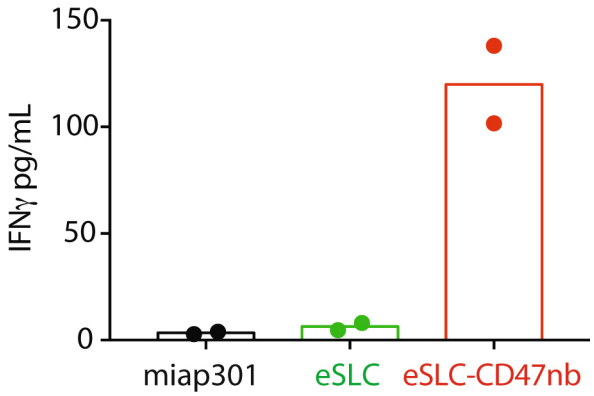


**Extended Data Fig. 7 | Immunotherapeutic bacteria lead to increased IFNγ production by splenic T cells after stimulation with tumor antigens.** Enzyme-linked immunosorbent assay (ELISA) of IFNγ using supernatants from overnight co-incubation of splenocytes isolated from each of the indicated treatment groups with irradiated A20 cells ($n = 2$ mice per group of three technical replicates).

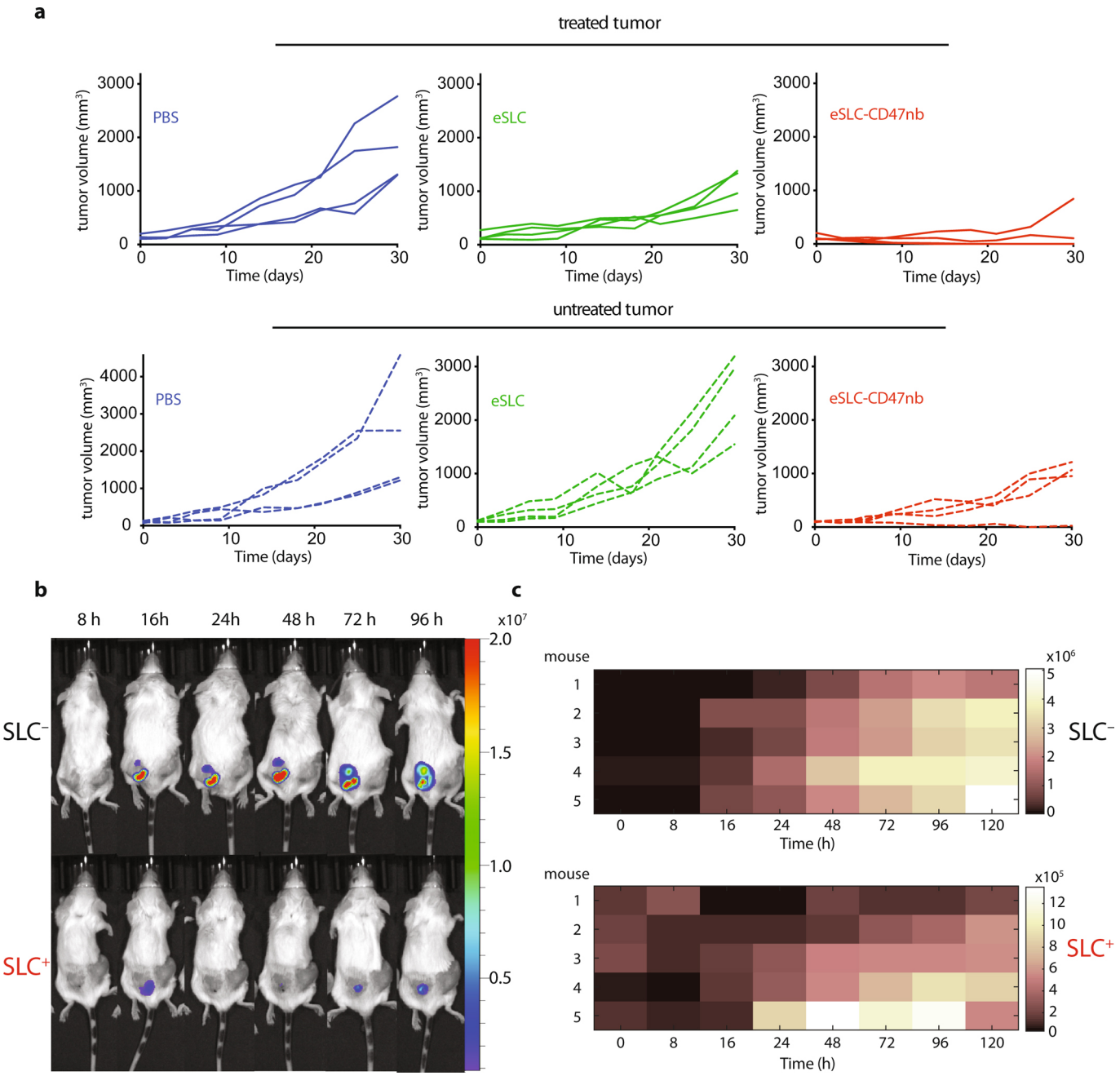


**Extended Data Fig. 8 | Intratumoral bacterial immunotherapy leads to distal tumor control. a**, Individual tumor growth trajectories of treated (injected) and untreated A20 tumors after intratumoral injection of PBS, eSLC or eSLC–CD47nb; related to Fig. 4a,b. **b**, SLC⁻ and SLC⁺ *E. coli* NisLux were intratumorally injected into a single flank of A20-tumor-bearing mice (scale represents radiance ($p\,s^{-1}\,cm^{-2}\,sr^{-1}$)). Luminescence was measured over time using in vivo imaging. Representative image of mouse no. 3 from each group over time. **c**, Luminescence heat maps over time ($n = 5$ mice per group). Colors represent average radiance ($p\,s^{-1}\,cm^{-2}\,sr^{-1}$).

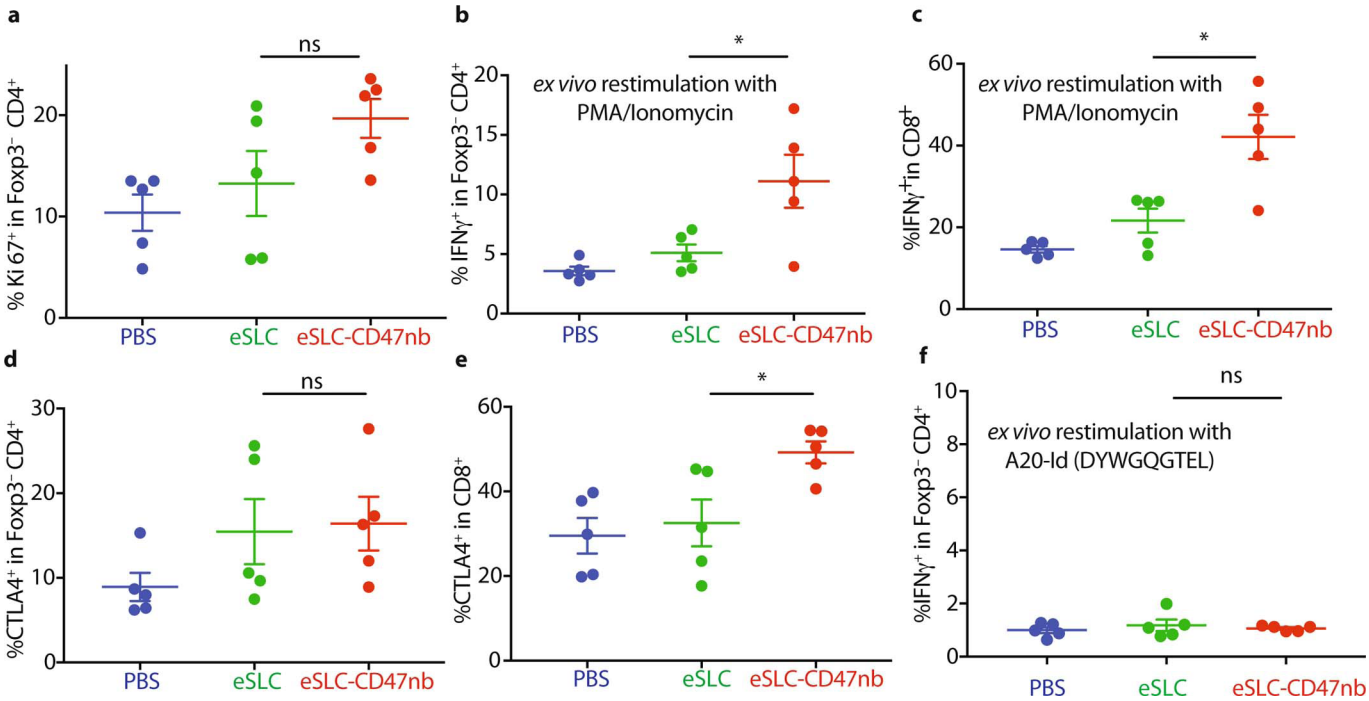


**Extended Data Fig. 9 | Immunophenotyping of tumor-infiltrating lymphocytes in untreated tumors after single-flank injection of bacteria.** First, $5 \times 10^6$ A20 cells were implanted into the hind flanks of BALB/c mice. Subsequently, when tumors reached ~100 $mm^3$ in volume (day 0), mice were treated with PBS, eSLC or eSLC–CD47nb on day 0, 4 and 7 by injection into a single tumor. Untreated tumors were extracted and analyzed by flow cytometry on day 8. $n = 5$ mice per group. **a**, Frequency of Ki-67$^+$ cells within the FOXP3$^-$CD4$^+$ T cell population ($P > 0.05$, unpaired two-tailed *t*-test). **b**,**c**, Frequency of tumor-infiltrating IFNγ$^+$ cells within the FOXP3$^-$CD4$^+$ T cell population (**b**; $^*P = 0.0327$, unpaired two-tailed *t*-test) and CD8$^+$ T cell population (**c**; $^*P = 0.0104$, unpaired two-tailed *t*-test) following ex vivo stimulation with PMA and ionomycin in the presence of brefeldin A. **d**,**e**, Frequencies of CTLA4$^+$ cells within the FOXP3$^-$CD4$^+$ T cell population (**d**; $P > 0.05$, unpaired two-tailed *t*-test) and CD8$^+$ T cell population (**e**; $^*P = 0.0259$, unpaired two-tailed *t*-test). **f**, Frequency of tumor-infiltrating IFNγ$^+$ cells within the FOXP3$^-$CD4$^+$ T cell population following ex vivo restimulation with A20-Id peptide (DYWGQGTEL) in the presence of brefeldin A ($P > 0.05$, unpaired two-tailed *t*-test). All data are mean ± s.e.m.

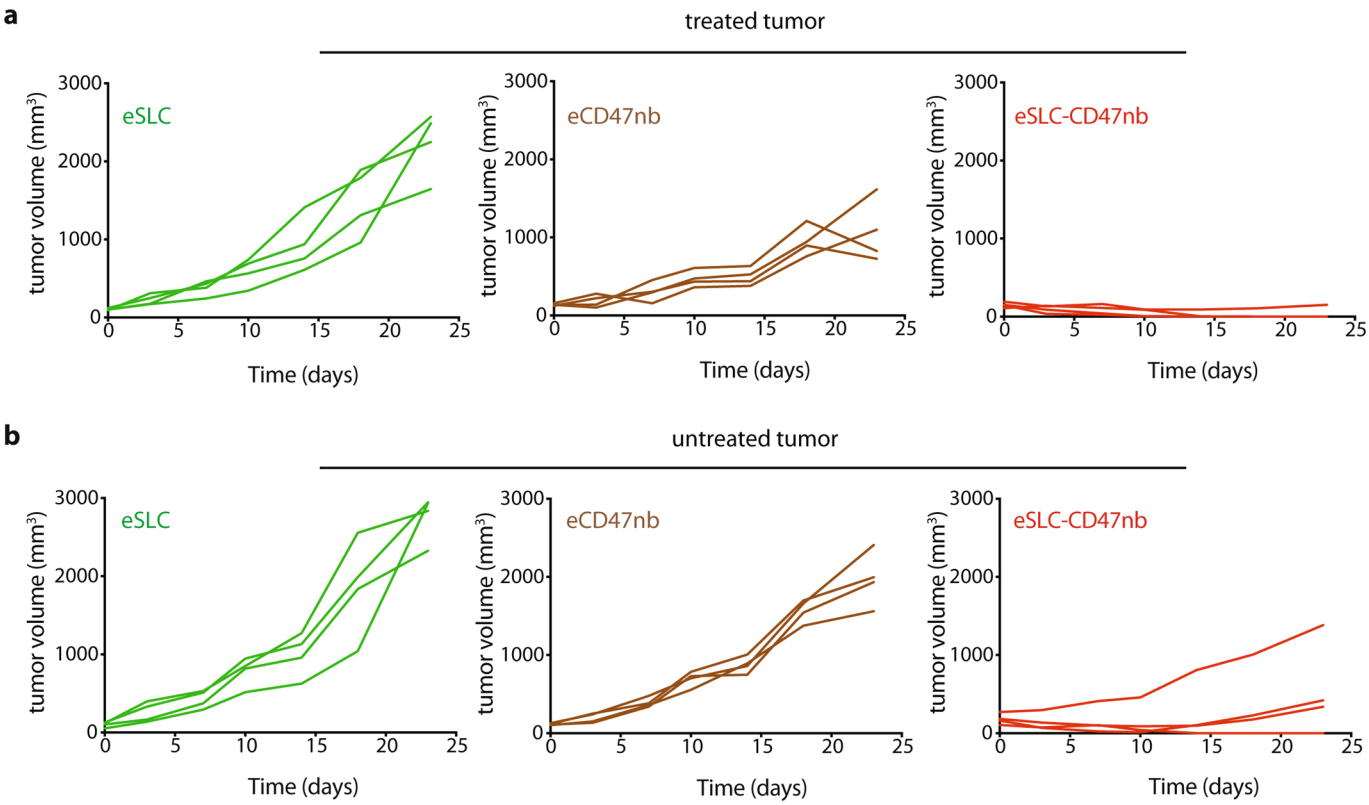


**Extended Data Fig. 10 | Distal tumor control requires SLC⁺ bacteria engineered to produce CD47nb. a**,**b**, Individual tumor growth trajectories of treated (injected) and untreated A20 tumors after intratumoral injection of eSLC, eCD47nb or eSLC–CD47nb ($n = 4$ mice per group); related to Fig. 4h,i.

nature research

Corresponding author(s): Tal Danino and Nicholas Arpaia

Last updated by author(s): May 19, 2019

# Reporting Summary

Nature Research wishes to improve the reproducibility of the work that we publish. This form provides structure for consistency and transparency in reporting. For further information on Nature Research policies, see Authors & Referees and the Editorial Policy Checklist.

## Statistics

For all statistical analyses, confirm that the following items are present in the figure legend, table legend, main text, or Methods section.

| n/a | Confirmed | |
|---|---|---|
| ☐ | ☒ | The exact sample size (*n*) for each experimental group/condition, given as a discrete number and unit of measurement |
| ☐ | ☒ | A statement on whether measurements were taken from distinct samples or whether the same sample was measured repeatedly |
| ☐ | ☒ | The statistical test(s) used AND whether they are one- or two-sided<br>*Only common tests should be described solely by name; describe more complex techniques in the Methods section.* |
| ☒ | ☐ | A description of all covariates tested |
| ☐ | ☒ | A description of any assumptions or corrections, such as tests of normality and adjustment for multiple comparisons |
| ☐ | ☒ | A full description of the statistical parameters including central tendency (e.g. means) or other basic estimates (e.g. regression coefficient) AND variation (e.g. standard deviation) or associated estimates of uncertainty (e.g. confidence intervals) |
| ☐ | ☒ | For null hypothesis testing, the test statistic (e.g. *F*, *t*, *r*) with confidence intervals, effect sizes, degrees of freedom and *P* value noted<br>*Give P values as exact values whenever suitable.* |
| ☒ | ☐ | For Bayesian analysis, information on the choice of priors and Markov chain Monte Carlo settings |
| ☒ | ☐ | For hierarchical and complex designs, identification of the appropriate level for tests and full reporting of outcomes |
| ☒ | ☐ | Estimates of effect sizes (e.g. Cohen's *d*, Pearson's *r*), indicating how they were calculated |

*Our web collection on statistics for biologists contains articles on many of the points above.*

## Software and code

Policy information about availability of computer code

| | |
|---|---|
| Data collection | FACS Diva v8.0 was used for flow cytometry data collection. |
| Data analysis | FlowJo v10 was used for analysis of flow cytometry data. GraphPad Prism v7.0 and v8.0 was used for statistical analysis. |

For manuscripts utilizing custom algorithms or software that are central to the research but not yet described in published literature, software must be made available to editors/reviewers. We strongly encourage code deposition in a community repository (e.g. GitHub). See the Nature Research guidelines for submitting code & software for further information.

## Data

Policy information about availability of data

All manuscripts must include a data availability statement. This statement should provide the following information, where applicable:

- Accession codes, unique identifiers, or web links for publicly available datasets
- A list of figures that have associated raw data
- A description of any restrictions on data availability

The data that support the findings of this study are available within the paper and its supplementary information files. Additional data are available from the authors upon reasonable request.

# Field-specific reporting

Please select the one below that is the best fit for your research. If you are not sure, read the appropriate sections before making your selection.

☒ Life sciences ☐ Behavioural & social sciences ☐ Ecological, evolutionary & environmental sciences

# Life sciences study design

All studies must disclose on these points even when the disclosure is negative.

| | |
|---|---|
| Sample size | We calculate sample size in our studies by using a power analysis and appropriate statistical test in G*Power 3.1 software. Previous animal studies, or small pilot studies when necessary, served as the basis for calculations of expected averages and deviations used to calculate power, for which we set experiment studies to a value of 0.8. This typically results in an experimental group size to be n = 4–7, depending on the experiment.<br>Sample size is explicitly stated for each experimental group for individual experiments in figure captions and data descriptions. |
| Data exclusions | No data were excluded. |
| Replication | All in vitro experiments were successfully repeated at least once. in vivo tumor experiments and immunophenotyping experiments were successfully repeated 2-3 times. |
| Randomization | The treatment groups were filled by randomly selecting from a pool of animals of comparable tumor volume at the beginning of all in vivo experiments. |
| Blinding | Investigators were not blinded to treatment groups. |

# Reporting for specific materials, systems and methods

We require information from authors about some types of materials, experimental systems and methods used in many studies. Here, indicate whether each material, system or method listed is relevant to your study. If you are not sure if a list item applies to your research, read the appropriate section before selecting a response.

## Materials & experimental systems

| n/a | Involved in the study |
|---|---|
| ☐ | ☒ Antibodies |
| ☐ | ☒ Eukaryotic cell lines |
| ☒ | ☐ Palaeontology |
| ☐ | ☒ Animals and other organisms |
| ☒ | ☐ Human research participants |
| ☒ | ☐ Clinical data |

## Methods

| n/a | Involved in the study |
|---|---|
| ☒ | ☐ ChIP-seq |
| ☐ | ☒ Flow cytometry |
| ☒ | ☐ MRI-based neuroimaging |

## Antibodies

| | |
|---|---|
| Antibodies used | Anti-mouse antibodies used for flow cytometry (clone, dilution, supplier, cat#)<br>anti-B220 BUV496 (RA3-6B2, 1:400, BD, 564662), anti-CD4 BV510 (RM4-5, 1:400, BioLegend, 100553), anti-CD8a PE-TexasRed (53-6.7, 1:400, BioLegend, 100761), anti-NKp46 BV605 (29A1.4, 1:200, BD, 137619), anti-Gr-1 PE (RB6-8C5, 1:400, Tonbo, 50-5931) anti-CD11b BV510 (M1/70, 1:400, BD, 562950), anti-F4/80 PE-eFluor610 (BM8, 1:400, eBioscience, 61-4801-82) anti-SIRPa PerCP-Cy5.5 (P84, 1:200, BioLegend, 144010), anti-MHC Class II (I-A/I-E) redFluor710 (M5/114.15.2, 1:800, Tonbo, 80-5321-U100), anti-CD3e PE-Cy7 (145-2C11, 1:400, Tonbo, 60-0031-U100), anti-TCRb BV711 (H57-597, 1:400, BD, 563135), anti-CTLA4 PE (UC10-4B9, 1:400, eBioscience, 12-1522-82), anti-Foxp3 FITC (FJK-16s, 1:400, eBioscience, 11-5773-82), anti-Ki-67 AF700 (SolA15, 1:400, Thermo, 56-5698-82), anti-Granzyme-B APC (QA16A02, 1:400, Biolegend, 372204), anti-IL-17A eFluor450 (eBio17B7, 1: 400, eBioscience, 48-7177-82), anti-TNF-a APC (MP6-XT22, 1: 400, eBioscience, 17-7321-82), anti-IFN-g PE (XMG1.2, 1:400, Tonbo, 50-7311-U100), anti-CD47 FITC (miap301, 1:200, BioLegend, 127504) |
| Validation | Antibodies used in this study were validated by manufactures and used according to supplied instructions. In certain cases, antibodies were re-validated and appropriate dilutions were determined by titration on ex vivo naive and activated splenocytes. |

## Eukaryotic cell lines

Policy information about cell lines

| | |
|---|---|
| Cell line source(s) | A20 murine lymphoma ( ATCC: TIB 208), 4T1 mammary carcinoma (ATCC: CRL 2539), B16-F10 murine melanoma (ATCC: CRL6475) |
| Authentication | Cell lines purchased from ATCC were frozen at early passage, thus did not require additional authentication. |
| Mycoplasma contamination | All cell lines tested negative for mycoplsma contamination. |
| Commonly misidentified lines (See ICLAC register) | No commonly misidentified cell lines were used. |

## Animals and other organisms

Policy information about studies involving animals; ARRIVE guidelines recommended for reporting animal research

| | |
|---|---|
| Laboratory animals | 4-8 week old BALB/c females or C57BL/6 females were purchased from Taconic Biosciences for in vivo experiments. |
| Wild animals | This study did not involve wild animals |
| Field-collected samples | This study did not involve samples collected from the field. |
| Ethics oversight | All animal experiments were approved by the Institutional Animal Care and Use Committee (Columbia University, protocol AC-AAAN8002 and AC-AAAZ4470). |

Note that full information on the approval of the study protocol must also be provided in the manuscript.

## Flow Cytometry

### Plots

Confirm that:

☒ The axis labels state the marker and fluorochrome used (e.g. CD4-FITC).

☒ The axis scales are clearly visible. Include numbers along axes only for bottom left plot of group (a 'group' is an analysis of identical markers).

☒ All plots are contour plots with outliers or pseudocolor plots.

☒ A numerical value for number of cells or percentage (with statistics) is provided.

### Methodology

| | |
|---|---|
| Sample preparation | Lymphocytes were isolated from tumor tissue by mechanical homogenization of tumor tissue followed and digestion with collagenase A (1 mg/ml; Roche) and DNase I (0.5 µg/ml; Roche) in isolation buffer (RPMI 1640 supplemented with 5% FBS, 1% l-glutamine, 1% pen-strep and 10 mM Hepes) for 1 hour at 37°C. Cells were filtered through 100 µm cell strainers, washed in isolation buffer and stained. Dead cells were excluded by staining with Ghost Dye cell viability reagent. |
| Instrument | BD LSRFortessa, FACS Diva v8 |
| Software | FlowJo v10 |
| Cell population abundance | Depends upon treatment - clearly identifiable by conventional flow cytometric approaches following tumor digestion. |
| Gating strategy | Gating of isolated TILs was performed following exclusion of B220+ A20 tumor cells; followed by identification of TCRb+ CD3+ NK1.1– prior to gating for CD4+ and CD8+ subpopulations. |

☐ Tick this box to confirm that a figure exemplifying the gating strategy is provided in the Supplementary Information.